© 2017. Published by The Company of Biologists Ltd | Development (2017) 144, 708-719 doi:10.1242/dev.138909

RESEARCH ARTICLE

Cell division and cadherin-mediated adhesion regulate lens epithelial cell movement in zebrafish

Toshiaki Mochizuki, Yi-Jyun Luo, Hsieh-Fu Tsai, Akane Hagiwara and Ichiro Masai*

ABSTRACT

In vertebrates, lens epithelial cells cover the anterior half of the lens fiber core. During development, lens epithelial cells proliferate, move posteriorly and differentiate into lens fiber cells after passing through the equator. To elucidate the mechanisms underlying lens epithelial cell movement, we conducted time-lapse imaging of zebrafish lens epithelium. Lens epithelial cells do not intermingle but maintain their relative positions during development. Cell division induces epithelial rearrangement, which subsequently promotes cell movement towards the equator. These data suggest that cell division is the major driving force for cell movement. In zebrafish, E-cadherin is expressed in lens epithelium, whereas N-cadherin is required for lens fiber growth. E-cadherin reduced lens epithelial cell movement, whereas N-cadherin enhanced it. Laser ablation experiments revealed that lens epithelium is governed by pulling tension, which is modulated by these cadherins. Thus, cell division and cadherin-mediated adhesion regulate lens epithelial cell movement via modulation of epithelial tension.

KEY WORDS: Cadherin, Cell movement, Epithelium, Lens, Tension, Zebrafish

INTRODUCTION

Cell proliferation is a key regulator of tissue morphogenesis (Gillies and Cabernard, 2011). In the *Drosophila* wing disc, high proliferation in the central region increases anisotropic mechanical tension in the peripheral region, which subsequently orients cell division and tissue growth (LeGoff et al., 2013; Mao et al., 2013). Tension-oriented cell division reduces tissue tension and facilitates tissue spreading during zebrafish gastrulation (Campinho et al., 2013). These examples indicate that cell proliferation and epithelial tension cooperatively shape tissue growth. However, mechanisms that coordinate cell proliferation and epithelial tension for tissue shaping remain to be elucidated.

In the vertebrate lens, lens epithelium covers the anterior half of the lens fiber core. During development, lens epithelial cells proliferate and move towards the periphery of the lens epithelium, called the equator (Hanna and O'Brien, 1961). At the equator, lens epithelial cells start to differentiate into lens fiber cells (McAvoy, 1978). Thus, cell proliferation and movement towards the equator are important for lens fiber growth. However, several interesting issues have not been addressed. For example, to keep a spheroid shape during lens growth, spatial and temporal frequencies at which lens epithelial cells pass through the equator must be equal around the equatorial circumference. However, it is unknown whether cell division density is radially uniform in the lens epithelium and, if not, how the same rate of cell movement at the equator is ensured. Quantitative and theoretical analyses on lens epithelial cell proliferation in mice was applied to understand the mechanism that regulates the size and shape of the lens during its growth (Shi et al., 2015; Šikić et al., 2015). However, cellular dynamics in the lens epithelium are largely unknown.

Classic studies using chick and mammalian lenses revealed that cell proliferation is low in the anterior region and high in the peripheral region of lens epithelium. This highly proliferative peripheral region is called the germinative zone (McAvoy, 1978; Modak et al., 1968; Zhou et al., 2006). We have established a zebrafish transgenic line that visualizes cell-cycle phases, and found a similar, highly proliferative zone in peripheral lens epithelium of zebrafish (Mochizuki et al., 2014). Furthermore, cell division orientation is biased longitudinally in the anterior region and circumferentially in the peripheral region of lens epithelium, suggesting a spatial pattern of cell division orientation. Although the FGF-Ras-MAPK pathway is required for active cell proliferation in the germinative zone in mice (Upadhya et al., 2013), it is unclear how cell proliferation and cell division orientation are spatially regulated and how these spatial patterns influence cell movement.

Here, we have conducted time-lapse imaging of lens epithelium using a zebrafish transgenic line that visualizes cell-cycle phases. Lens epithelial cells do not intermingle but maintain their relative positions during development. Furthermore, cell division triggers epithelial rearrangement, which subsequently promotes cell movement towards the equator. Thus, cell division is a major force for cell movement. In vertebrates, E-cadherin is expressed in lens epithelium, whereas N-cadherin is required for lens fiber growth (Mochizuki et al., 2014; Pontoriero et al., 2009; Xu et al., 2002). E-cadherin reduced cell movement, whereas N-cadherin enhanced it. A laser ablation experiment revealed that lens epithelium is governed by pulling tension, which is modulated by these cadherins. Thus, cell division and cadherin-mediated cell adhesion regulate lens epithelial cell movement by modulating epithelial tension.

RESULTS

Cell division promotes cell movement in lens epithelium

We conducted time-lapse imaging of lens epithelium from 33-45 h post-fertilization (hpf), using a zebrafish transgenic line *Tg(h2afva:GFP; EF1α:mCherry-zGem)*, which visualizes cell nuclei and cell-cycle phases (Mochizuki et al., 2014) (Fig. 1A). First, we focused on the anterior lens epithelium, which covers the region from the anterior pole to the anterior border of the germinative zone (60 cells at 33 hpf, Fig. 1B and Movie 1). During the scanned period, lens epithelial cells did not intermingle, but maintained their relative

Developmental Neurobiology Unit, Okinawa Institute of Science and Technology Graduate University, 1919-1 Tancha, Onna, Okinawa 904-0495, Japan.

*Author for correspondence (masai@oist.jp)

T.M., 0000-0001-6401-5605; Y.-J.L., 0000-0002-3418-3146; H.-F.T., 0000-0002-8652-4643; I.M., 0000-0002-6626-6595

Received 25 April 2016; Accepted 4 January 2017

Development (2017) 144, 708-719 doi:10.1242/dev.138909

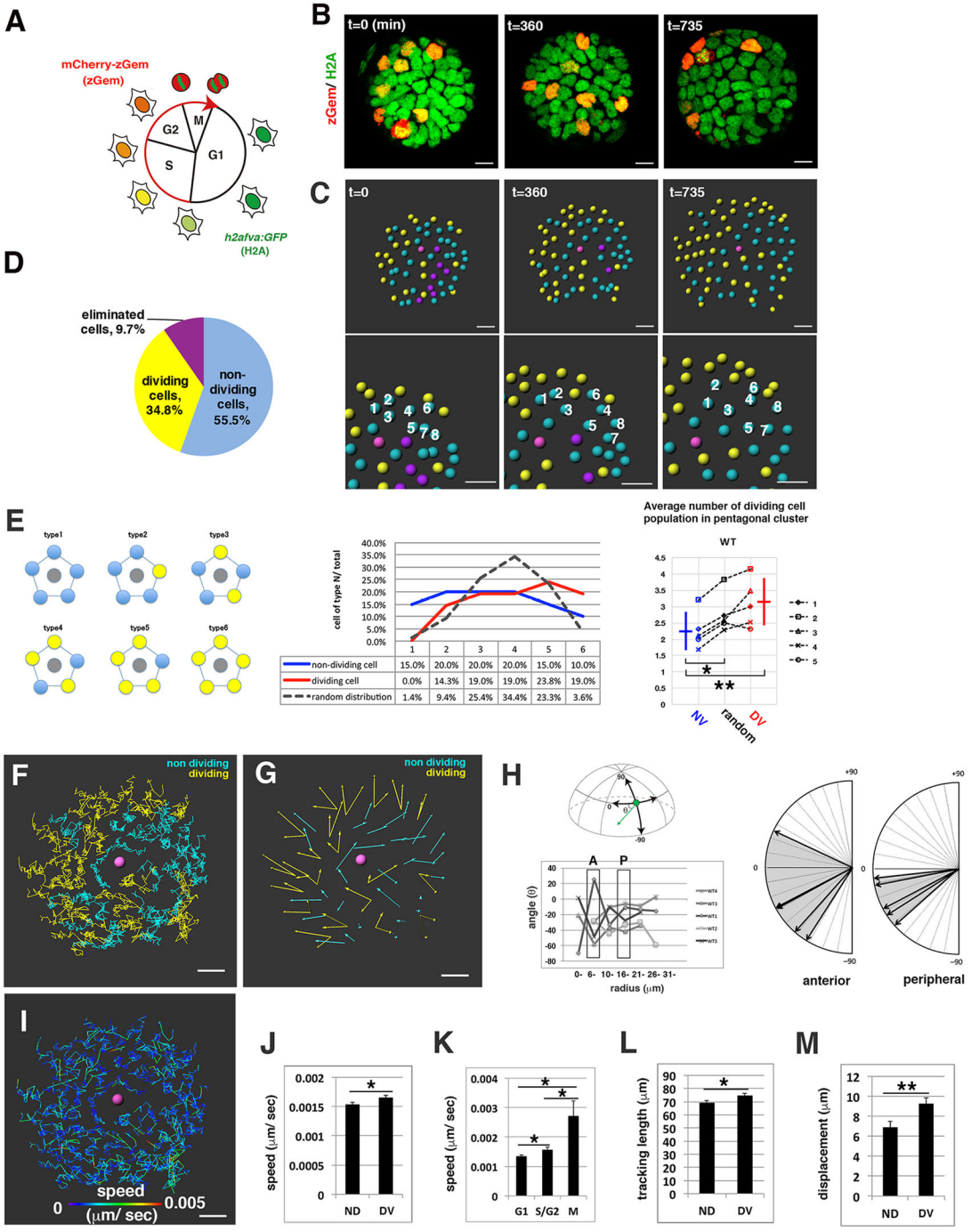

Fig. 1. Cell movement of wild-type anterior lens epithelium. (A) Fluorescence pattern of *Tg(h2afva:GFP; EF1α:mCherry-zGem)*. Adapted, with permission, from Mochizuki et al. (2014). (B) Anterior views of lens epithelium of *Tg(h2afva:GFP; EF1α:mCherry-zGem)*. Time indicates the time elapsed after 33 hpf. This lens is designated as WT1. (C) (Upper) Schematics of images shown in B. Yellow, blue and purple indicate dividing, non-dividing and eliminated cell populations, respectively. (Lower) Enlarged views of upper panels. The numbers indicate individual cells in the non-dividing cell cluster. (D) Average percentages of non-dividing, dividing and eliminated cell populations in five wild-type lenses at 33 hpf. (E) (Left) Six pentagonal patterns consisting of non-dividing (blue) and dividing (yellow) cell populations. (Middle) Distribution of pentagonal patterns of WT1 at 45 hpf. The broken gray line indicates the estimated profile of pentagonal patterns when non-dividing and dividing cell populations are randomly selected. Blue and red lines indicate the profiles of pentagonal patterns, in which non-dividing and dividing cell populations are in pentagonal centers. Non-dividing and dividing cell populations tend to assemble with the same cell type. (Right) Average number of dividing cell population in non-dividing cell population-centered (blue), dividing cell population-centered (red) pentagonal clusters and random distribution model (black). Values of five wild-type lenses are plotted. Averages and s.d. are indicated by horizontal and vertical bars, respectively. (F,G) Trajectory (F) and displacement (G) in WT1. (H) Cell movement direction along the AP axis for five wild-type lenses. (Left) AP position is defined by the lens sphere radius: r=0 (anterior) to 31 μm (equator). Cell movement direction is defined by the angle (θ) between the displacement vector and the circumferential axis: θ=–90 (longitudinal) to 0 (circumferential). (Right) Cell movement direction in anterior and peripheral regions, which correspond to squares marked A and P. The range of cell movement becomes more narrow in peripheral region than in the anterior region. (I) Speed of cell movement in WT1. (J,L,M) Average speed (J), tracking length (L) and displacement (M) of non-dividing (ND) and dividing (DV) cell populations in WT1. (K) Average speed of G1, S/G2 and M phase cells in WT1. Data in J-M are mean±s.e.m. Student's *t*-test: **P*<0.05, ***P*<0.01. Scale bars: 10 μm.

Development (2017) 144, 708-719 doi:10.1242/dev.138909

positions, pushing each other back and forth. Cell division mainly induces surrounding cells to move.

Lens epithelial cells are classified into three groups: during the 12 h scanned period, the first group did not undergo cell division (Fig. 1C, blue). The second group underwent one round of cell division (Fig. 1C, yellow), and the third group disappeared due to cell death or movement into lens fiber area (Fig. 1C, purple). Hereafter, these three groups are designated as the non-dividing cell population, the dividing cell population and the eliminated cell population. The average fractions of non-dividing, dividing, and eliminated cell populations in five wild-type lenses, which are designated WT1-WT5, at 33 hpf were 55.5, 34.8 and 9.7%, respectively (Fig. 1D, Fig. S1A–E); thus, more than 50% of anterior lens epithelial cells did not divide during the 12 h scan. In the eliminated cell population, 84.6% were associated with the collapse of chromatin, whereas 15.4% moved into lens fiber area, suggesting that cell death is a major cause of cell elimination (Fig. S2A).

Interestingly, non-dividing and dividing cell populations were spatially segregated (Fig. 1C, upper panels). Using another zebrafish transgenic line, *Tg(h2afva:GFP; EF1α:mCherry-CAAX)*, which visualizes cell nuclei and plasma membranes, we observed that cell division often occurred sequentially within neighboring cells, which led to clustering of their daughter cells (Fig. S2B; Movie 2). Furthermore, non-dividing cell clusters maintained their associations and moved as cell assemblies (Fig. 1C, lower panels). To examine whether clustering of dividing and non-dividing cell populations is significant, we selected five adjacent cells surrounding each lens epithelial cell and examined the profile of six pentagonal cluster types, which consist of different combinations of dividing and non-dividing cell populations (Fig. 1E, left). We compared distributional profiles of pentagonal clusters, in which dividing and non-dividing cell populations were in the center, with the estimated profile under a random distribution model (see supplementary Materials and Methods). In wild-type lenses, both dividing and non-dividing cell population-centered pentagonal clusters tend to contain the same cell type (Fig. 1E, middle). Average number of dividing cell population in dividing cell population-centered clusters was significantly higher than that of non-dividing cell population-centered clusters (Fig. 1E, right), supporting the observation that both dividing and non-dividing cell populations tend to cluster with the same cell type. We also examined pentagonal patterns of cells pre-designated as dividing or non-dividing cell population at the initial (t=0 min) and middle point (t=360 min) of the scanned period (Fig. S3A-B). The pentagonal distribution pattern of both populations was less segregated from that of the random distribution model at t=0 and 360 than at t=735 (Fig. S3C), suggesting that dividing and non-dividing cell populations became segregated during development, probably through clustered cell divisions.

Next, we examined the trajectory of cell movement (Fig. 1F) and cell displacement (Fig. 1G). The spatial movement pattern was variable in the anterior region among individual lenses; however, the movement direction was circumferentially biased in the peripheral region in wild-type lenses (Fig. 1H). The circumferential shift of cell movement in the peripheral region correlates with the spatial pattern of cell division orientation (Mochizuki et al., 2014), suggesting that cell division promotes cell movement.

We further examined three parameters of cell movement: speed (Fig. 1I), total tracking length and displacement. We compared the speed of the dividing cell population with that of the non-dividing cell population in the lens shown in Fig. 1C, namely WT1 (as a wild-type representative lens). On average, the dividing cell population moved faster than the non-dividing cell population (Fig. 1J). We also compared cell movement speed in different cell cycle phases of all lens epithelial cells. Cells in M phase moved markedly faster than cells in G1 or S/G2 phase (Fig. 1K). Tracking length (Fig. 1L) and displacement (Fig. 1M) were longer in the dividing cell population than in the non-dividing cell population. Displacement was roughly 10% of tracking length (Fig. 1M), supporting the observation that cells pushed each other back and forth without forward movement. We confirm a similar tendency with regard to speed, tracking, and displacement in five wild-type lenses, including WT1 (Fig. 2A-C), although the difference of tracking length was less significant between dividing and non-dividing cell population (P=0.074, Fig. 2B). Thus, cell division promotes cell movement in lens epithelium.

E-cadherin suppresses cell movement in the anterior lens epithelium

E-cadherin (Cdh1) is expressed in lens epithelium. We previously examined a hypomorphic allele of zebrafish E-cadherin mutant, *half baked*^{rk3} (*hab*^{rk3}), and reported that the spatial pattern of cell division orientation was affected, although lens epithelial cell proliferation and lens fiber differentiation are generally normal (Mochizuki et al., 2014). In mouse E-cadherin mutants, epithelial-to-mesenchymal transition (EMT) occurs in lens epithelium after postnatal stages (Pontoriero et al., 2009). However, such EMT was not observed in the *hab*^{rk3}mutant until 96 hpf (data not shown).

To determine the role of E-cadherin in cell movement, we conducted time-lapse scanning of lens epithelium of the same allele of E-cadherin mutant, *hab*^{rk3}, combined with the transgenic line *Tg(h2afva:GFP; EF1α:mCherry-zGem)* from 33 to 45 hpf (Fig. 3A; Movie 3). The average fraction of non-dividing, dividing, and eliminated cell populations in three *hab*^{rk3} mutant lenses, which are designated E-cad1 to E-cad3 (Fig. S1F), at 33 hpf were 64.9, 22.6, and 12.4%, respectively (Fig. S1A). In the *hab*^{rk3} mutant, the non-dividing and dividing cell fractions were higher and lower than in wild type, respectively (Fig. S1B,C), although their difference was less significant. The eliminated cell fraction was not different (Fig. S1D). However, in the *hab*^{rk3} mutant, the eliminated cell population that moved into the lens fiber area was 47.8%, higher than in wild type (Fig. S2A), suggesting that E-cadherin knockdown increases the fraction of cells that moved into lens fiber area. As in the wild type, non-dividing cells assembled and moved together during the scanned period (Fig. 3B; Movie 3). However, both dividing and non-dividing cell population-centered pentagonal clusters showed a distribution pattern similar to that of the random distribution model in two of three *hab*^{rk3} mutant lenses, namely E-cad1 and E-cad2, during scanned period (Fig. 3C and Fig. S3A,B). In the remaining *hab*^{rk3} mutant lens, namely E-cad3, the dividing cell population was spatially localized in a one-sided peripheral area (Fig. S3F), so pre-designated dividing and non-dividing cell populations were already segregated at 33 hpf (Fig. S3A,B). Even in this situation, the average number of dividing cell population in pentagonal clusters was not significantly different between dividing and non-dividing cell population-centered clusters in *hab*^{rk3} mutant lenses (Fig. S3C), suggesting that dividing and non-dividing cell populations fail to be segregated.

Next, we examined the trajectory of cell movement (Fig. 3D) and cell displacement (Fig. 3E) in the *hab*^{rk3} mutant. The displacement pattern was less coordinated in the *hab*^{rk3} mutant than in the wild type (Fig. 3E). Cell movement direction was significantly less circumferential in the peripheral region of *hab*^{rk3} mutant lenses (Figs 2D and 3F). Next, we examined speed, tracking length and

Development (2017) 144, 708-719 doi:10.1242/dev.138909

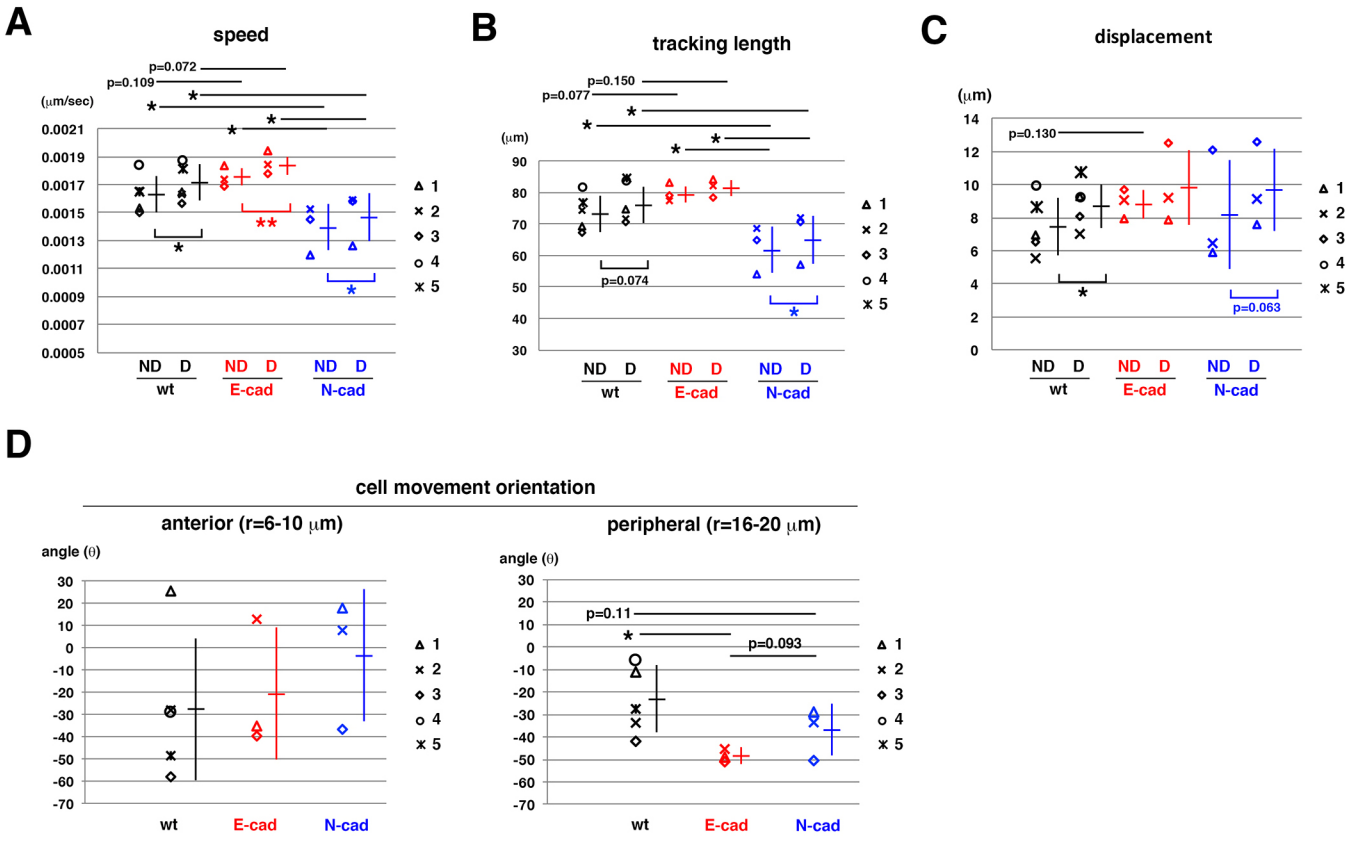

Fig. 2. Cell movement parameters of wild-type, E-cadherin mutant and N-cadherin morphant lenses. (A-D) Speed (A), tracking length (B), displacement length (C), cell movement direction (D) of anterior lens epithelial cells. Values of five wild-type, three E-cadherin mutant and three N-cadherin morphant lenses are plotted. ND and DV in A-C indicate non-dividing and dividing cell populations, respectively. Cell movement angle in the anterior zone (r=6-10 μm) and the peripheral zone (r=16-20 μm) are indicated in the left and right panels. Averages and s.d. are indicated by horizontal and vertical bars, respectively. Probabilities were calculated using Student's *t*-test: **P*<0.05. *P*-values less than 0.15 are also indicated. Images of wild-type, E-cadherin mutant and N-cadherin morphant lenses numbered with a 1 (WT1, E-cad1 and N-cad1) are shown in Figs 1B, 3A and 4A, respectively.

displacement of a *hab*^{rk3} mutant lens shown in Fig. 3A, namely E-cad1 (as an E-cadherin mutant representative lens), and compared with those of the wild-type representative lens, WT1. The average speed of all lens epithelial cells was faster in E-cad1 than in WT1 (Fig. 3G,H), and both dividing and non-dividing cell populations contributed to this increased speed (Fig. 3I). Movement of G1 phase cells was significantly faster in E-cad1 than in WT1, whereas the speed of S/G2 and M phase cells did not differ between E-cad1 and WT1 (Fig. 3J), suggesting that movement is enhanced mainly in G1 phase in the *hab*^{rk3} mutant. Average tracking length of all lens epithelial cells was longer in E-cad1 than in WT1 (Fig. 3K). Longer tracking length was observed in both dividing and non-dividing cell populations in E-cad1 (Fig. 3L). By contrast, average displacement of all lens epithelial cells was similar between WT1 and E-cad1 (Fig. 3M). Displacement of non-dividing and dividing cell populations was also similar between WT1 and E-cad1 (Fig. 3N). These data suggest that E-cadherin suppresses cell movement in the anterior lens epithelium.

We compared five wild-type and three *hab*^{rk3} mutant lenses, including WT1 and E-cad1. Average speed and tracking length were slightly higher in the *hab*^{rk3} mutant than in wild type for both dividing and non-dividing cell population, although their differences were less significant (0.05<*P*<0.15, Fig. 2A,B). Average displacement of non-dividing cell population in the *hab*^{rk3} mutant was slightly higher than in wild type (*P*=0.13), but displacement of dividing cells was not different from that of wild type (Fig. 2C). Thus, cell movement speed is faster in the E-cadherin mutant than in wild type, but faster speed does not correlate with longer displacement, especially for a dividing cell population.

Cell movement in the equatorial region

In wild type, cell movement direction is circumferentially biased in peripheral lens epithelium (Fig. 1H). At the equator, cells start to differentiate into lens fibers, which elongate along the anteroposterior (AP) axis of the lens sphere. We conducted time-lapse imaging of the equatorial region of wild-type lenses from 33 to 45 hpf, using *Tg(h2afva:GFP; EF1α:mCherry-zGem)* (Fig. S4A, upper panels; Movie 4). We focused on seven cell rows covering the equatorial region along the AP axis (Fig. S4A, lower panels), and examined their trajectories and displacements (Fig. S4B). Cells located anterior to the equator moved circumferentially, whereas cells in or posterior to the equator moved posteriorly. Thus, cell movement direction changes at the equator (Fig. S4E).

Next, we examined equatorial cell movement in the *hab*^{rk3} mutant (Fig. S4C,D; Movie 5). As in the wild type, cell movement direction changes at the equator in the *hab*^{rk3} mutant (Fig. S4E). We also examined speed, tracking length and displacement in the equatorial region. In wild-type lenses, speed and tracking length gradually increased along the AP axis (Fig. S4F,G), and displacement increased markedly after cells pass through the equator (Fig. S4H). In the *hab*^{rk3} mutant, speed and tracking length corresponded to the highest part of the wild-type range

Development (2017) 144, 708-719 doi:10.1242/dev.138909

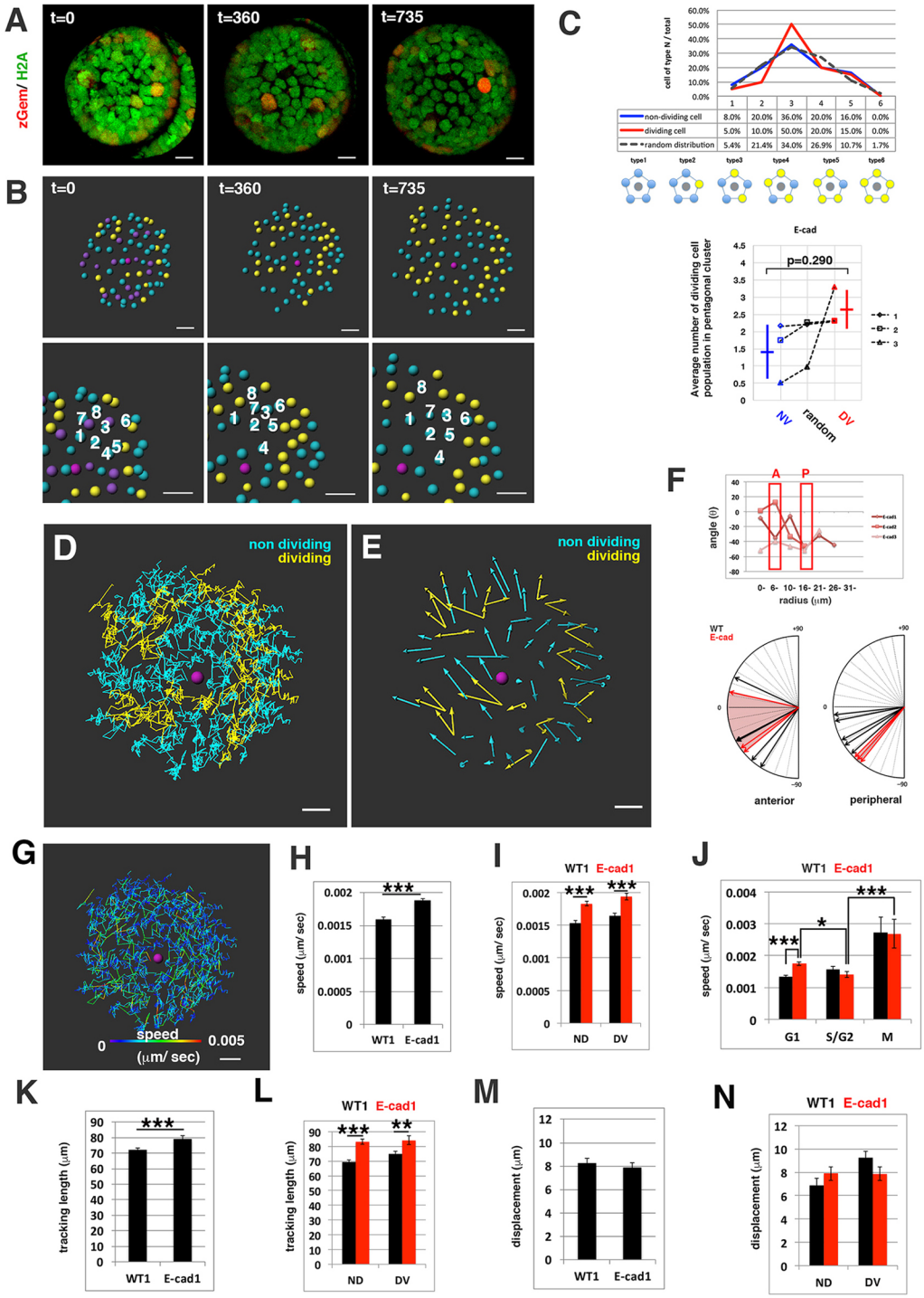

Fig. 3. Cell movement in anterior lens epithelium of the E-cadherin mutant. (A) *hab*^{rk3} mutant lens epithelium combined with *Tg(h2afva:GFP; EF1α:mCherry-zGem)*. This lens is designated as E-cad1. (B) (Upper) Schematics of images shown in A. Yellow, blue and purple indicate dividing, non-dividing and eliminated cell populations, respectively. (Lower) Enlarged view of upper panels. Numbers indicate individual cells in the non-dividing cell cluster. (C) (Upper) Distribution of pentagonal patterns of E-cad1 at 45 hpf. Peaks of non-dividing and dividing cell populations are the same as that of the random distribution model, suggesting that dividing and non-dividing cell populations fail to segregate. (Bottom) Average number of dividing cell population in non-dividing cell population-centered (blue), dividing cell population-centered (red) pentagonal clusters and random distribution model (black). Values of three *hab*^{rk3} mutant lenses are plotted. E-cad1 is indicated by the number 1. Averages and s.d. are indicated by horizontal and vertical bars, respectively. (D,E) Trajectory (D) and displacement (E) of cell movement in E-cad1. (F) (Upper) Cell movement direction in three *hab*^{rk3} mutant lenses. A and P indicate anterior and peripheral regions, respectively. (Bottom) Cell movement direction in anterior and peripheral regions, which correspond to squares marked A and P, in wild-type (black arrows, shown in Fig. 1H) and *hab*^{rk3} mutant lenses (red arrows). The range of cell movement direction of the *hab*^{rk3} mutant is indicated in red and is less circumferential than that of the wild type in the peripheral region. (G) Speed of cell movement on trajectory of E-cad1. (H,K,M) Cell movement speed (H), tracking length (K) and displacement (M) of all lens epithelial cells in WT1 and E-cad1. (I,L,N) Cell movement speed (I), tracking length (L) and displacement (N) of non-dividing (ND) and dividing (DV) cell populations in E-cad1 (red) and WT1 (black). (J) Cell movement speed of G1, S/G2 and M phase cells in Ecad1 (red) and WT1 (black). The error bars in H-N indicate s.e.m. Student's *t*-test: **P*<0.05, ***P*<0.01, ****P*<0.005. Scale bars: 10 μm.

Development (2017) 144, 708-719 doi:10.1242/dev.138909

(Fig. S4F,G), whereas displacement was highly variable (Fig. S4H). Thus, E-cadherin mutant cells move faster than wild-type cells in the equatorial region, but higher speed did not correlate with longer displacement.

N-cadherin promotes cell movement in the anterior lens epithelium

In chick, N-cadherin (Cdh2) promotes lens fiber differentiation, by complexing with α-catenin and actin filaments (Leonard et al., 2011). We also reported that N-cadherin is required for lens fiber elongation in zebrafish (Masai et al., 2003). Consistently, zebrafish N-cadherin was expressed in lens epithelium, but more intensely in elongating lens fiber cells (Fig. S5A). Here, we injected a morpholino antisense oligo against N-cadherin (MO-Ncad) at low concentrations. This induced typical N-cadherin mutant defects, such as failure of neural tube closure (Fig. S5B), but did not grossly affect lens epithelial cell proliferation and lens fiber differentiation (Fig. S5C,D). In the N-cadherin morphant, the lens fiber core was smaller than in wild-type lenses, but the number of lens epithelial cells was not altered (Fig. S5E). Thus, low doses of MO-Ncad reduces only the size of the lens fiber core.

Next, we conducted time-lapse imaging of lens epithelium of the N-cadherin morphant, combined with *Tg(h2afva:GFP; EF1α:mCherry-zGem)* from 33 to 45 hpf (Fig. 4A; Movie 6). The average fractions of non-dividing, dividing and eliminated cell populations in three N-cadherin morphant lenses [which are designated N-cad1 to N-cad3 (Fig. S1G)] at 33 hpf were 49.8, 40.4 and 9.8%, respectively (Fig. S1A), values that are not significantly different from wild type (Fig. S1B-D). In contrast to the *hab*^{rk3} mutant, 94.7% of eliminated cells were associated with cell death in the N-cadherin morphant, whereas only 5.3% of eliminated cells moved into the lens fiber area (Fig. S2A). Non-dividing and dividing cell populations became spatially segregated to form clusters in the N-cadherin morphant during development (Fig. 4B, upper panels). Furthermore, non-dividing cell clusters moved as cell assemblies during the scanned period (Fig. 4B, lower panels). Interestingly, non-dividing and dividing cell population clusters were more segregated in the N-cadherin morphant than in wild type at 45 hpf (Fig. 4C). We examined the formation of non-dividing and dividing cell population clusters in the N-cadherin morphant during development (Fig. S3A, B). The average number of dividing cell population was significantly higher in dividing cell population-centered clusters and lower in non-dividing cell population-centered clusters than in the random distribution model after t=360 min (Fig. S3C), suggesting that segregation of dividing and non-dividing cell populations is enhanced in the N-cadherin morphant.

Next, we examined trajectories of cell movement (Fig. 4D) and cell displacement (Fig. 4E) in N-cadherin morphant lenses. Cell movement direction was less biased circumferentially in the peripheral region, although the difference between wild-type and N-cadherin morphant was less significant (P=0.11) (Figs 2D and 4F). We examined speed (Fig. 4G), tracking length and displacement in the N-cadherin morphant. We compared a N-cadherin morphant lens shown in Fig. 4A, namely N-cad1 and the representative wild-type lens WT1. The average speed of all lens epithelial cells was slower in N-cad1 than in WT1 (Fig. 4H), and the slower speed was observed in both dividing and non-dividing cell populations (Fig. 4I). Speeds of G1 and S/G2 cells were significantly lower in N-cad1 than in WT1, whereas the speed of M-phase cells was not significantly different (Fig. 4J). Average tracking length of all lens epithelial cells was shorter in N-cad1 than in WT1 (Fig. 4K), and the shorter tracking length was observed in both non-dividing and dividing cell populations (Fig. 4L). Average displacement of all lens epithelial cells was shorter in N-cad1 than in WT1 (Fig. 4M). However, the shorter displacement was significant only in dividing cell populations (Fig. 4N). These data suggest that N-cadherin promotes cell movement in the anterior lens epithelium.

We compared five wild-type lenses with three N-cadherin morphant lenses, including WT1 and N-cad1. In the N-cadherin morphant, average speed and tracking length were significantly lower than those of wild type for dividing and non-dividing cell populations (Fig. 2A,B). However, displacement was not different between wild type and the N-cadherin morphant (Fig. 2C). This is partly because one of three N-cadherin morphant lenses, N-cad3, showed exceptionally high displacement (Fig. 2C). We examined the spatial pattern of displacement (Fig. S6). In WT1 and N-cad1, cells with high displacements (>15 µm) were few and were located in the peripheral region. By contrast, many peripheral cells showed high displacement (>15 µm) in N-cad3. These peripheral cells are the primary dividing cell population that moved *en masse* toward the equator (Fig. S6). Such large clustered cell divisions near the equator may increase displacement length, regardless of lower speed. Thus, speed is slower, but slower speed does not correlate with shorter displacement in the N-cadherin morphant.

N-cadherin suppresses cell movement toward the equator

We conducted time-lapse scanning of the equatorial region in N-cadherin morphant lenses combined with *Tg(h2afva:GFP; EF1α:mCherry-zGem)* (Fig. S7A, upper panels; Movie 7). We focused on seven cell rows covering the equatorial region (Fig. S7A, lower panels). Cell trajectories (Fig. S7B) and the spatial profile of cell movement direction (Fig. S7C) indicate that all rows of cells moved posteriorly in the N-cadherin morphant. Speed, tracking length and displacement increased in the N-cadherin morphant compared with wild type (Fig. S7D-F). In contrast to the anterior lens epithelium, N-cadherin prevents cell movement in the peripheral region.

Epithelial tension is reduced in E- and N-cadherin knockdown lenses

In general, cadherin-mediated cell adhesion counterbalances epithelial tension. To clarify lens epithelial tension, we used a laser to ablate single cells in the anterior lens epithelium of the transgenic line *Tg(h2afva:GFP; EF1α:mCherry-CAAX)*, and performed time-lapse imaging to examine the temporal change of the ablated area from 15 s before ablation to 255 s post-ablation. In 50 hpf wild-type lenses, the ablated area initially increased to a maximum at 30 s post-ablation, and progressively decreased thereafter (Fig. 5A,B). Initial expansion of the ablated area was isotropic (data not shown). We examined actomyosin contraction, which represents healing processes associated with epithelial damage (Abreu-Blanco et al., 2011, 2012), using a zebrafish transgenic line *Tg(actb1:myl12.1-eGFP; EF1α:mCherry-CAAX)*, which visualizes myosin 2 and cell membranes (Behrndt et al., 2012). In wild type, myosin 2 accumulated beneath cell membranes adjacent to the ablated area by 99 s post-ablation (Fig. S8; Movie 8), suggesting that initial expansion and later shrinkage of the ablated area depend on physical tension and on actomyosin-mediated healing, respectively. Initial expansion of the ablated area suggests that wild-type lens epithelial cells pull each other.

In *hab*^{rk3} mutant lenses, the ablated area did not increase after ablation (Fig. 5A,C,E), suggesting that epithelial tension is low. Furthermore, the ablated area failed to shrink after 30 s post-ablation

Development (2017) 144, 708-719 doi:10.1242/dev.138909

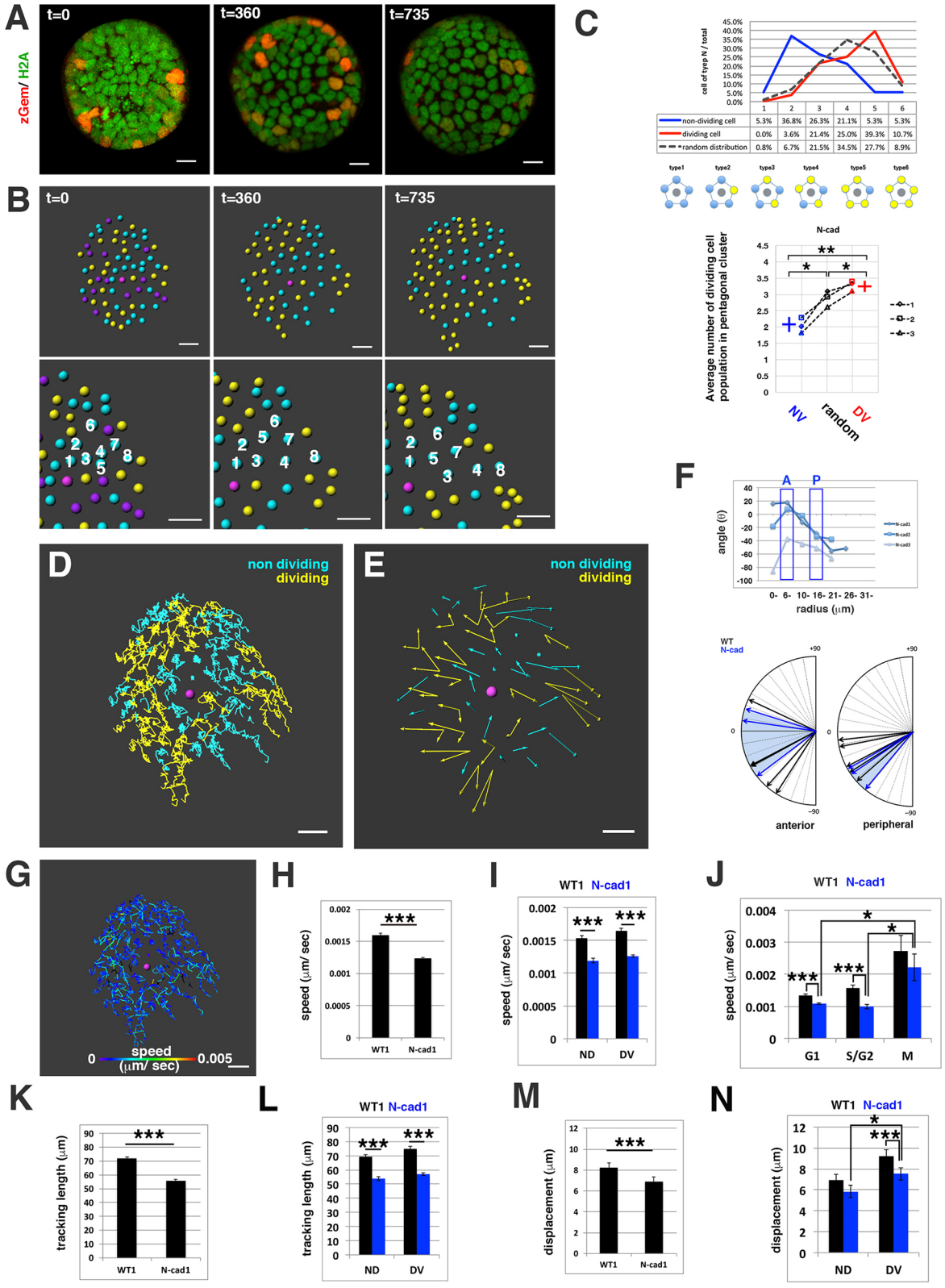

Fig. 4. See next page for legend.

(Fig. 5C,F), suggesting that healing requires E-cadherin. Interestingly, in the E-cadherin morphant, myosin 2 accumulation was slower than in wild type, and proceeded irregularly in patches (Fig. S8; Movie 9).

In N-cadherin morphant lenses, the ablated area did not expand after ablation (Fig. 5A,D,E), suggesting that epithelial tension is low. Later shrinkage of the ablated space normally proceeded after 30 s post-ablation (Fig. 5D,F), suggesting that healing does not

Development (2017) 144, 708-719 doi:10.1242/dev.138909

Fig. 4. Cell movement in anterior lens epithelium of the N-cadherin morphant. (A) N-cadherin morphant lens epithelium combined with *Tg (h2afva:GFP; EF1α:mCherry-zGem)*. This lens is designated as N-cad1. (B) (Upper) Schematics of images shown in A. Yellow, blue and purple indicate dividing, non-dividing and eliminated cell populations, respectively. (Lower) Enlarged view of upper panels. Numbers indicate individual cells in the non-dividing cell cluster. (C) (Upper) Distribution of pentagonal patterns of N-cad1 at 45 hpf. A peak shift is observed in both non-dividing and dividing cell populations. Furthermore, the segregation level is more prominent in the N-cadherin morphant. (Bottom) Average number of dividing cell population in non-dividing cell population-centered (blue), dividing cell population-centered (red) pentagonal clusters and random distribution model (black). Values of three N-cadherin morphant lenses are plotted. N-cad1 is indicated by the number 1. Averages and s.d. are indicated by horizontal and vertical bars, respectively. (D,E) Trajectory (D) and displacement (E) of cell movement in N-cad1. (F) (Upper) Cell movement direction in three N-cadherin morphant lenses. A and P indicate the anterior and peripheral regions, respectively. (Bottom) Cell movement direction in anterior and peripheral regions, corresponding to squares marked A and P, in wild-type (black arrows, shown in Fig. 1H) and N-cadherin morphant lenses (blue arrows). The range of cell movement direction of N-cadherin morphants is indicated in blue and is less circumferential than that of the wild type in the peripheral region. (G) Speed of cell movement on trajectory of N-cad1. (H,K,M) Cell movement speed (H), tracking length (K) and displacement (M) of all lens epithelial cells in WT1 and N-cad1. (I,L,N) Cell movement speed (I), tracking length (L) and displacement (N) of non-dividing (ND) and dividing (DV) cell populations in N-cad1 (blue) and WT1 (black). (J) Cell movement speed of G1, S/G2 and M phase cells in N-cad1 (blue) and WT1 (black). The error bars in H-N indicate the s.e.m. Student's *t*-test: **P*<0.05, ***P*<0.01, ****P*<0.005. Scale bars: 10 µm.

require N-cadherin. In the N-cadherin morphant, myosin 2 accumulation was initiated with normal timing (Fig. S8; Movie 10), but proceeded irregularly in patches, as with the E-cadherin morphant.

Apical cell size, and perhaps nuclear volume, are influenced by the balance between epithelial tension and cell adhesion. Previously, we reported that the perimeter length of lens epithelial cells is longer in the E-cadherin mutant than in wild type (Mochizuki et al., 2014). We found that the apical size of anterior lens epithelial cells was larger in the *hab*^{rk3} mutant and smaller in the N-cadherin morphant at 50 hpf (Fig. 5G). We also measured nuclear volumes of lens epithelial cells. Nuclear volume was more variable in the *hab*^{rk3} mutant than in wild type, whereas it was significantly lower in the N-cadherin morphant than in wild type (Fig. S9).

Cell division triggers cell intercalation, which subsequently promotes cell movement

Cell division is likely to relax epithelial tension, enabling surrounding cells to move towards the equator. To clarify the relationship between cell division, epithelial rearrangement and cell movement, we examined their temporal profiles in lens epithelium. Using time-lapse imaging of anterior lens epithelium in wild-type transgenic line *Tg(h2afva:GFP; EF1α:mCherry-CAAX)* (Fig. S2B), we focused on a particular area consisting of 10-15 lens epithelial cells. In wild type, cell division often occurred sequentially in short time windows, followed by cell intercalation (Fig. 6A, Fig. S10A,B). Thus, the period of cell division was segregated from that of cell intercalation. We further calculated the rate of area expansion per scanned frame and sorted it into three periods: cell division, cell intercalation and the rest period when no cell division or cell intercalation occurred (Fig. 6C, Fig. S10E-F). The average rate of area expansion of three wild-type lenses (Fig. 6E) was 0.090 (% of original area size/min) for the cell-division period, but 0.234 (%/min) for the cell-intercalation period, which is twice higher than that of the cell-division period. Interestingly, the expansion rate was −0.015 (%/min) during the rest period. These data suggest that cell division itself does not promptly increase the area, but later cell intercalation increases the area accompanied with cell movement.

Next, we examined temporal profiles of cell division, cell intercalation and lens epithelial area size in the *hab*^{rk3} mutant. In contrast to wild type, cell intercalation often occurred during the cell division period (Fig. 6B; Fig. S10C,D). We calculated the rate of area expansion per scanned frame (Fig. 6D; Fig. S10G,H). The average area expansion rate of three *hab*^{rk3} mutant lenses (Fig. 6E) was 0.181, 0.154 and 0.179 (%/min) for periods of cell division, cell intercalation and rest, respectively. These data suggest that expansion rate increases during the cell division period in the *hab*^{rk3} mutant, although the *hab*^{rk3} mutant showed more individual variation. Furthermore, continuous enlargement occurs during the rest period in the *hab*^{rk3} mutant. Overlapping of cell division and cell intercalation periods indicate that the reduction of cell adhesion allows surrounding cells to move immediately after cell division. Thus, E-cadherin suppresses intercalation of surrounding cells neighbor to cell division, resulting in temporal segregation of cell division and cell intercalation periods. Furthermore, E-cadherin inhibits expansion of the apical areas of lens epithelial cells during the rest period.

DISCUSSION

In this study, we conducted time-lapse imaging of lens epithelium using zebrafish, and found several interesting traits of lens epithelial cells. First, lens epithelial cells are classified into dividing and non-dividing cell populations. These two populations are spatially segregated during development. Second, in non-dividing cell clusters, cells do not intermingle, but move as cell assemblies. Third, cell movement direction is biased circumferentially in the peripheral lens epithelium, similar to cell division orientation, indicating a correlation between cell division and cell movement. Finally, cell division triggers cell intercalation, which subsequently promotes cell movement. Thus, cell division is a major driving force for cell movement in lens epithelium.

Cell division triggers cell intercalation, which promotes lens epithelial cell movement

As both cell movement direction and cell division orientation are similarly biased to the circumferential direction in the peripheral lens epithelium in zebrafish, we initially assumed that cell division simply generates directional cell movement, as previously reported for zebrafish gastrulation (Gong et al., 2004) and *Drosophila* germband extension (da Silva and Vincent, 2007). However, the case of zebrafish lens is more complex. Cell division often occurred sequentially within neighboring cells, resulting in clustering of dividing cells. Furthermore, the non-dividing cell population did not intermingle, but moved as a cell assembly. Thus, it is likely that expansion of dividing cell clusters promotes collective movement of neighboring non-dividing cells. Intriguingly, clustered cell divisions do not overlap temporally with cell intercalation, and the expansion rate of lens epithelial area is higher during the cell interaction period than during cell division period. These observations suggest that cell division does not drive prompt movement of surrounding cells, but induces cell intercalation, which subsequently promotes cell movement.

An interesting question is how are dividing cell populations clustered? In wild-type lens, dividing and non-dividing cell populations are gradually segregated during development, suggesting that cell division promotes clustering of these two cell populations. Furthermore, these two cell populations failed to segregate in the E-cadherin mutant. As the fraction of dividing cells is reduced in the E-cadherin mutant, decreased cell division may delay cluster formation. The second possibility is that segregation of

Development (2017) 144, 708-719 doi:10.1242/dev.138909

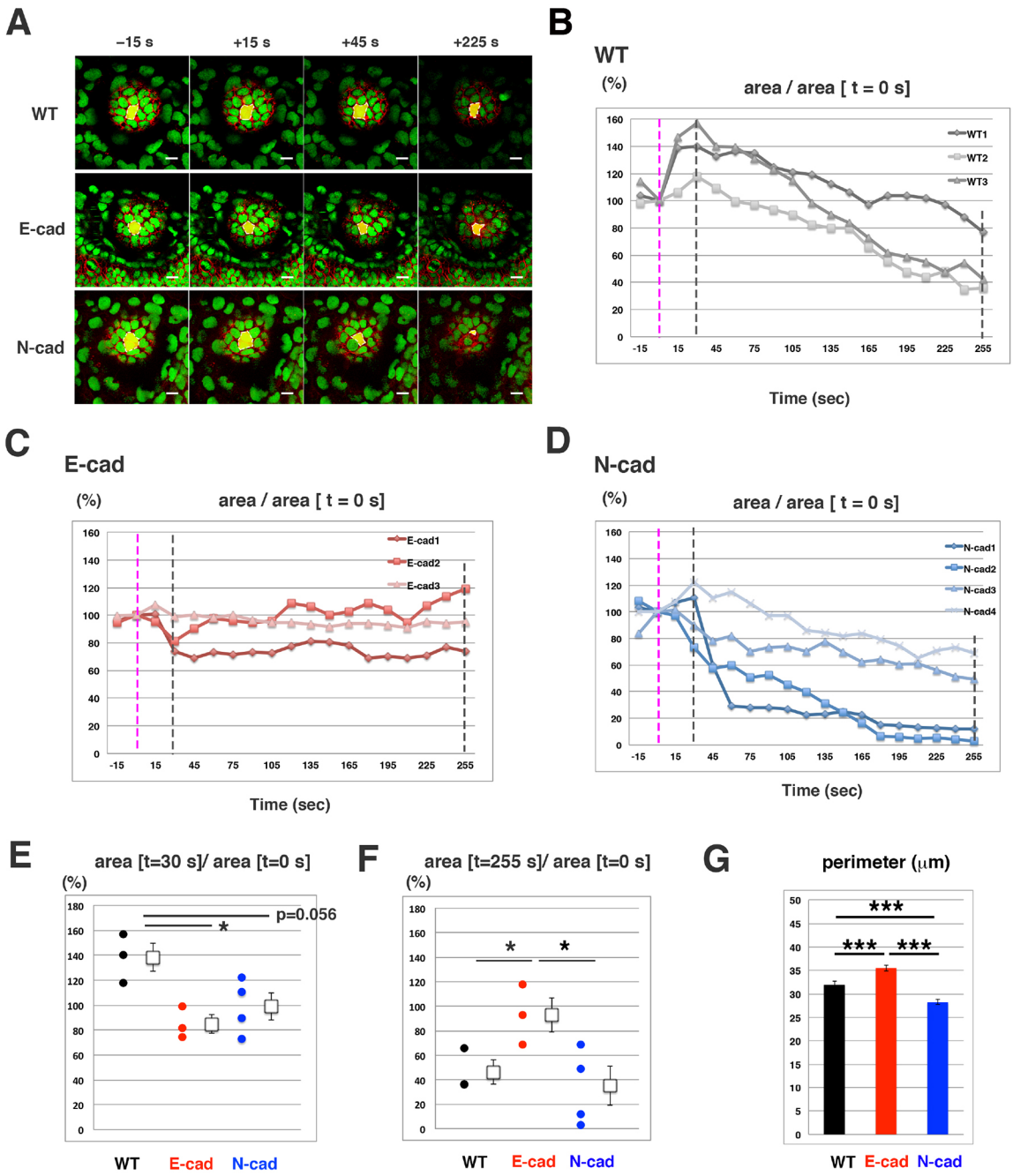

Fig. 5. Laser ablation of lens epithelial cells. (A) Time lapse scanning of 50 hpf wild-type, E-cadherin mutant and N-cadherin morphant lenses. Time indicates the time elapsed after laser ablation. Ablated cells are indicated in green. (B-D) Temporal profile of the ablated area at 50 hpf wild-type (B), E-cadherin mutant (C) and N-cadherin morphant (D) lenses. Ablated areas are normalized by the initial area at t=0 (pink dotted line). Black dotted lines indicate the time when the ablated area reaches its peak in the wild type (t=30) as well as the time at the end of scanning (t=255). (E,F) The ablated area at t=30 (E) and t=255 (F) relative to the initial area at t=0. (G) Perimeter length of wild-type, E-cadherin mutant and N-cadherin morphant lenses at 50 hpf. The error bars indicate the s.e.m. Student's *t*-test: **P*<0.05, ****P*<0.005. Scale bars: 10 μm.

dividing and non-dividing cell populations is not maintained in the E-cadherin mutant. In general, cell intercalation is regulated by remodeling of adherens junctions, which requires dynamic, but stable, coupling with E-cadherin and myosin 2 accumulation (Bardet et al., 2013; Levayer and Lecuit, 2013). As cell intercalation occurs abnormally during the cell division period in the E-cadherin mutant, loss of adherens junctions in the E-cadherin mutant may lead to improper epithelial remodeling, which disrupts clustering of non-dividing cells.

It was reported that rat kidney epithelial cells show stochastically pulsed MAPK activation *in vitro*, the frequency of which correlates with cell proliferation rate (Aoki et al., 2013). Interestingly, this pulsed MAPK activity is propagated to neighbor cells through EGF/Ras/MAPK signaling pathways. A similar propagation mechanism of cell proliferation may underlie clustering of cell division in zebrafish lens epithelium. Given that the frequency of MAPK activity pulses depends on cell density (Aoki et al., 2013), it would be interesting to investigate whether the level of cell proliferation

Development (2017) 144, 708-719 doi:10.1242/dev.138909

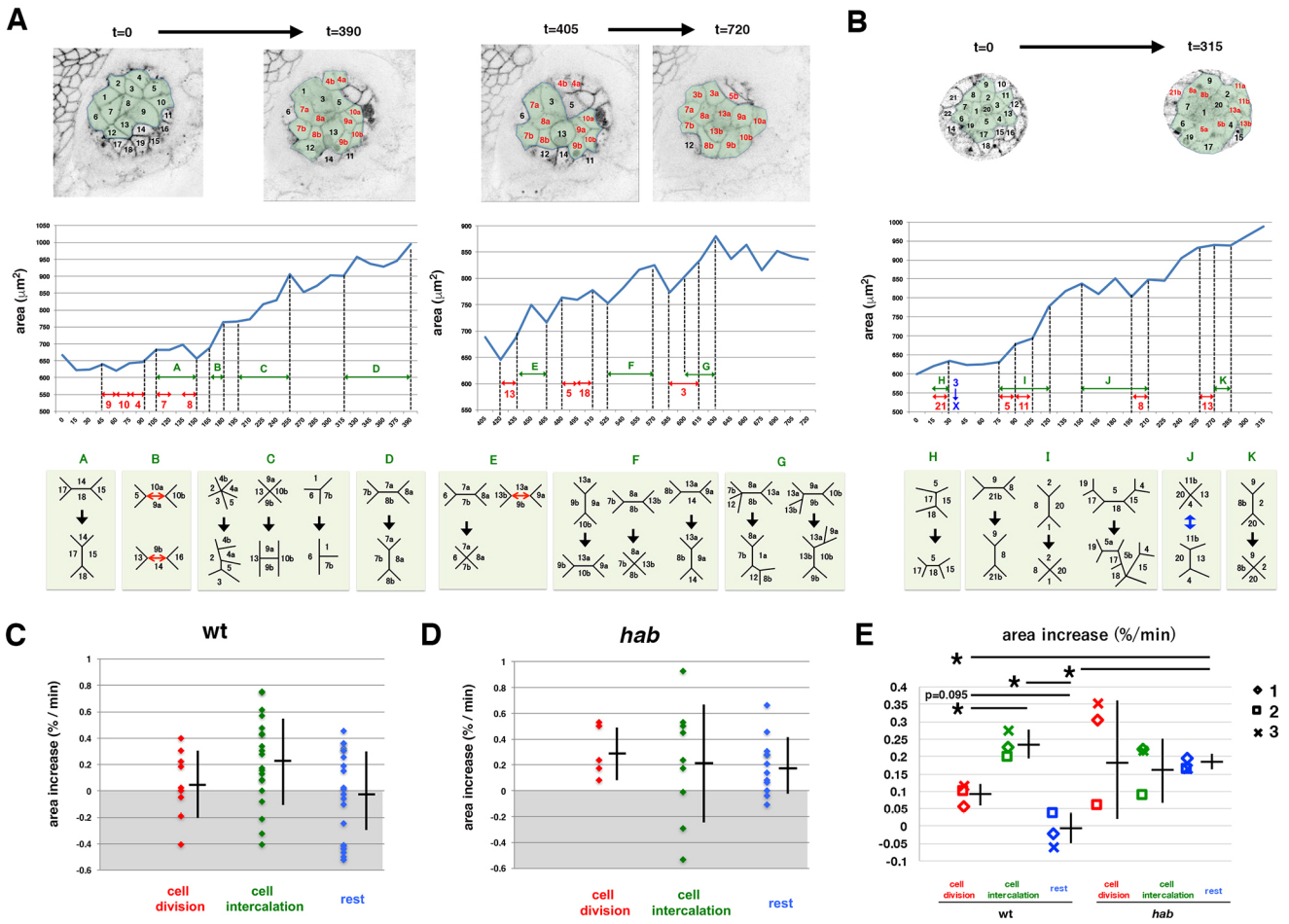

Fig. 6. Temporal profile of lens epithelial expansion of the wild type and the E-cadherin mutant. (A) Wild-type lens epithelial area, consisting of 12 cells during the first 390 min (left panels) and 10 cells during the last 315 min (right panels). The top panels indicate the composition of individual lens epithelial cells. Divided daughter cells are in red. Middle panels display temporal profiles of the area. Red and green arrows indicate cell division events and periods when cell intercalation occurred, respectively. Bottom panels indicate cell intercalation that occurred in the corresponding period of middle panels. (B) Temporal change of *hab*^{rk3} mutant lens epithelial area consisting of 14 cells during the first 315 min. (C,D) Expansion rate per time frame of lens epithelial area of wild-type (C) and *hab*^{rk3} mutant (D) lens shown in A and B, respectively, during periods of cell division (red), cell intercalation (green) and the rest period (blue). Averages and s.d. are indicated by horizontal and vertical bars, respectively. The average value of the cell intercalation period is higher than others in wild type, whereas average values are similar during all three periods in *hab*^{rk3} mutant. (E) The average rate of lens epithelial expansion in three wild-type and *hab*^{rk3} mutant lenses. Averages and s.d. are indicated by horizontal and vertical bars, respectively. Although values of cell division period in the *hab*^{rk3} mutant are variable, profiles were similar to those shown in C and D. Student's *t*-test: **P*<0.05.

depends on epithelial tension. Epithelial tension is transmitted through adherens junctions via E-cadherin (Borghi et al., 2012; Yonemura et al., 2010). A smaller dividing cell population in the E-cadherin mutant may indicate that higher tension promotes cell proliferation in zebrafish lens epithelium.

Cadherins regulate cell movement through epithelial tension

Speed of lens epithelial cell movement is increased in E-cadherin mutant, but decreased in N-cadherin morphant. Our laser ablation experiments show that lens epithelial cells pull each other, and that such pulling tension is reduced in both E-cadherin mutant and N-cadherin morphant. As N-cadherin is required for lens fiber elongation (Masai et al., 2003), defects in this process may affect the interface structure between the lens epithelium and lens fiber core, which physically reduces lens epithelial cell movement in the N-cadherin morphant. Alternatively, lower epithelial tension may cause slower cell movement in the N-cadherin morphant. Because lens epithelium covers the anterior half of the lens fiber core, the growth of the lens fiber core promoted by N-cadherin may increase tensile force on the lens epithelium, which E-cadherin-dependent cell adhesion counterbalances to preserve as elastic energy (Fig. S11A). As E-cadherin is required for actomyosin accumulation underneath plasma membranes (Levayer and Lecuit, 2013), irregular and patchy accumulation of myosin 2 in response to laser ablation suggests that E-cadherin-mediated cell adhesion, which balances with epithelial tension in equilibrium, becomes lower in the N-cadherin morphant. In this case, epithelial tension generated by lens fiber growth is decreased in the N-cadherin morphant, resulting in slower cell movement and smaller apical cell and nuclear size (Fig. S11B).

However, the situation in the E-cadherin mutant is complex. Although N-cadherin-generated tensile force may be intact in the E-cadherin mutant, E-cadherin mutant epithelium could not preserve epithelial tension in the lens epithelium because of the loss of adherens junctions. Furthermore, E-cadherin mutant cells are likely to have increased fluidity of cell movement. By sudden removal of single cells using laser ablation in the E-cadherin mutant, surrounding cells could not sense tension from neighboring cells

Development (2017) 144, 708-719 doi:10.1242/dev.138909

but just filled the ablated space because of increased cell fluidity (Fig. S11B). The fraction of cell division is decreased in E-cadherin mutant lens epithelium, which may reduce epithelial tension by the delay of lens fiber growth. Reduction of lens epithelial cell number and higher flexibility of cell shape may explain increased apical cell size in E-cadherin mutant. Loss of adherens junction may compromise force transmission from plasma membranes to nuclear membranes, which would contribute to variable nuclear size. Further investigation is required to fully address molecular mechanisms that induce these E-cadherin mutant phenotypes.

In summary, our findings suggest that E-cadherin and N-cadherin cooperatively regulate lens epithelial cell movement by modulating epithelial tension. Epithelial tension is a key mediator that links cell division and cell movement in zebrafish lens epithelium.

MATERIALS AND METHODS

Zebrafish strains

Zebrafish (*Danio rerio*) were maintained as described previously (Westerfield, 1993). OIST wild type, *oki*, zebrafish *e-cadherin/cdh1* mutant, *half baked*$^{hab^{rk3}}$ (Shimizu et al., 2005) and the transgenic lines *Tg(EF1α:mCherry-zGem)*^{oki011} (Mochizuki et al., 2014), *Tg(h2afva:GFP)*$^{kca6/kca66}$ (Pauls et al., 2001), *Tg(EF1α:mCherry-CAAX)*^{oki049} and *Tg(actb1:myl12.1-eGFP)* (Behrndt et al., 2012) were used. Animal care and experimental protocols were approved by the OIST Institutional Animal Care and Use Committee.

Tg(EF1α:mCherry-CAAX) transgenic line

The CAAX domain of zebrafish hrasa (NM_001017263) fused to mCherry was subcloned into a Tol2 transposon-based expression vector, pT2AL200R150G (Urasaki et al., 2006). This DNA construct was injected into fertilized eggs with Tol2 transposase mRNA, to establish a transgenic line, namely *Tg(EF1α:mCherry-CAAX)*.

Morpholino

Morpholino antisense oligos against *n-cadherin/cdh2* (MO-Ncad) and *e-cadherin/cdh1* (MO-Ecad) were designed as described previously [see ncad-MO1 in Lele et al. (2002) and MO3-cdh1 in Babb and Marrs (2004)]. MO-Ncad and MO-Ecad were injected into fertilized eggs at 50 and 20 µM, respectively.

Time-lapse imaging and image analyses

Time lapse images of zebrafish lens epithelium with the transgene *Tg(h2afva:GFP; EF1α:mCherry-zGem)* or *Tg(h2afva:GFP; EF1α:mCherry-CAAX)* were obtained using the confocal laser scanning microscope and analyzed using Imaris software (ver. 7.6.5, Bitplane). Detailed procedures are described in the supplementary Materials and Methods.

Laser ablation experiments

Single cells were ablated using a UV laser pulse and epithelial cells were scanned in time-lapse at 11-15 s intervals. Using Image-J software, the ablated area was analyzed. Detailed procedures are described in the supplementary Materials and Methods.

Determination of cell movement direction

Cell movement direction in the lens epithelium was calculated using time-lapse 3D images from an anterior view. Detailed procedures are described in the supplementary Materials and Methods.

Evaluation of clustering

Using images of *Tg(h2afva:GFP; EF1α:mCherry-zGem)*, we selected the five cells closest to the cell of interest, forming a virtual pentagonal of surrounding cells. Combinations of dividing and non-dividing cell numbers in pentagonal cell clusters were determined. Distribution profiles of pentagonal cluster patterns with a centered dividing cell population and a centered non-dividing cell population, and of the random distribution model were compared. Detailed procedures are described in the supplementary Materials and Methods.

Histology

Immunostaining was performed as described previously (Imai et al., 2010). Antibodies against Pax6 (Covance PRB-278P, 1:100), PCNA (clone PC10; Sigma, 1:100), Prox1 (GTX128354; Gene Tex, 1:500) and N-cadherin (GTX125885; Gene Tex, 1:100-200) were used.

Acknowledgements

We thank Atsushi Miyawaki for the mCherry-zGeminin plasmid, and Masahiko Hibi and Carl-Philipp Heisenberg for the zebrafish *hab*^{rk3} mutant and *Tg(actb1:myl12.1-eGFP)* transgenic lines, respectively. We thank Steven D. Aird for editing the manuscript.

Competing interests

The authors declare no competing or financial interests.

Author contributions

T.M. and I.M. designed the experiments, analyzed the data and prepared the manuscript. T.M. and Y.-J.L. performed time-lapse imaging experiments. T.M., H.-F.T. and A.H. performed laser ablation experiments.

Funding

This work was supported by an internal grant from the Okinawa Institute of Science and Technology Graduate University to I.M.

Supplementary information

Supplementary information available online at
http://dev.biologists.org/lookup/doi/10.1242/dev.138909.supplemental

References

Abreu-Blanco, M. T., Verboon, J. M. and Parkhurst, S. M. (2011). Cell wound repair in Drosophila occurs through three distinct phases of membrane and cytoskeletal remodeling. *J. Cell Biol.* **193**, 455-464.

Abreu-Blanco, M. T., Verboon, J. M., Liu, R., Watts, J. J. and Parkhurst, S. M. (2012). Drosophila embryos close epithelial wounds using a combination of cellular protrusions and an actomyosin purse string. *J. Cell Sci.* **125**, 5984-5997.

Aoki, K., Kumagai, Y., Sakurai, A., Komatsu, N., Fujita, Y., Shionyu, C. and Matsuda, M. (2013). Stochastic ERK activation induced by noise and cell-to-cell propagation regulates cell density-dependent proliferation. *Mol. Cell* **52**, 529-540.

Babb, S. G. and Marrs, J. A. (2004). E-cadherin regulates cell movements and tissue formation in early zebrafish embryos. *Dev. Dyn.* **230**, 263-277.

Bardet, P.-L., Guirao, B., Paoletti, C., Serman, F., Léopold, V., Bosveld, F., Goya, Y., Mirouse, V., Graner, F. and Bellaïche, Y. (2013). PTEN controls junction lengthening and stability during cell rearrangement in epithelial tissue. *Dev. Cell* **25**, 534-546.

Behrndt, M., Salbreux, G., Campinho, P., Hauschild, R., Oswald, F., Roensch, J., Grill, S. W. and Heisenberg, C.-P. (2012). Forces driving epithelial spreading in zebrafish gastrulation. *Science* **338**, 257-260.

Borghi, N., Sorokina, M., Shcherbakova, O. G., Weis, W. I., Pruitt, B. L., Nelson, W. J. and Dunn, A. R. (2012). E-cadherin is under constitutive actomyosin-generated tension that is increased at cell-cell contacts upon externally applied stretch. *Proc. Natl. Acad. Sci. USA* **109**, 12568-12573.

Campinho, P., Behrndt, M., Ranft, J., Risler, T., Minc, N. and Heisenberg, C.-P. (2013). Tension-oriented cell divisions limit anisotropic tissue tension in epithelial spreading during zebrafish epiboly. *Nat. Cell Biol.* **15**, 1405-1414.

da Silva, S. M. and Vincent, J.-P. (2007). Oriented cell divisions in the extending germband of Drosophila. *Development* **134**, 3049-3054.

Gillies, T. E. and Cabernard, C. (2011). Cell division orientation in animals. *Curr. Biol.* **21**, R599-R609.

Gong, Y., Mo, C. and Fraser, S. E. (2004). Planar cell polarity signalling controls cell division orientation during zebrafish gastrulation. *Nature* **430**, 689-693.

Hanna, C. and O'Brien, J. E. (1961). Cell production and migration in the epithelial layer of the lens. *Arch. Ophthalmol.* **66**, 103-107.

Imai, F., Yoshizawa, A., Fujimori-Tonou, N., Kawakami, K. and Masai, I. (2010). The ubiquitin proteasome system is required for cell proliferation of the lens epithelium and for differentiation of lens fiber cells in zebrafish. *Development* **137**, 3257-3268.

LeGoff, L., Rouault, H. and Lecuit, T. (2013). A global pattern of mechanical stress polarizes cell divisions and cell shape in the growing Drosophila wing disc. *Development* **140**, 4051-4059.

Lele, Z., Folchert, A., Concha, M., Rauch, G. J., Geisler, R., Rosa, F., Wilson, S. W., Hammerschmidt, M. and Bally-Cuif, L. (2002). parachute/n-cadherin is required for morphogenesis and maintained integrity of the zebrafish neural tube. *Development* **129**, 3281-3294.

Leonard, M., Zhang, L., Zhai, N., Cader, A., Chan, Y., Nowak, R. B., Fowler, V. M. and Menko, A. S. (2011). Modulation of N-cadherin junctions and their role as epicenters of differentiation-specific actin regulation in the developing lens. *Dev. Biol.* **349**, 363-377.

Development (2017) 144, 708-719 doi:10.1242/dev.138909

Levayer, R. and Lecuit, T. (2013). Oscillation and polarity of E-cadherin asymmetries control actomyosin flow patterns during morphogenesis. *Dev. Cell* **26**, 162-175.

Mao, Y., Tournier, A. L., Hoppe, A., Kester, L., Thompson, B. J. and Tapon, N. (2013). Differential proliferation rates generate patterns of mechanical tension that orient tissue growth. *EMBO J.* **32**, 2790-2803.

Masai, I., Lele, Z., Yamaguchi, M., Komori, A., Nakata, A., Nishiwaki, Y., Wada, H., Tanaka, H., Nojima, Y., Hammerschmidt, M. et al. (2003). N-cadherin mediates retinal lamination, maintenance of forebrain compartments and patterning of retinal neurites. *Development* **130**, 2479-2494.

McAvoy, J. W. (1978). Cell division, cell elongation and distribution of alpha-, beta- and gamma-crystallins in the rat lens. *J. Embryol. Exp. Morphol.* **44**, 149-165.

Mochizuki, T., Suzuki, S. and Masai, I. (2014). Spatial pattern of cell geometry and cell-division orientation in zebrafish lens epithelium. *Biol. Open* **3**, 982-994.

Modak, S. P., Morris, G. and Yamada, T. (1968). DNA synthesis and mitotic activity during early development of chick lens. *Dev. Biol.* **17**, 544-561.

Pauls, S., Geldmacher-Voss, B. and Campos-Ortega, J. A. (2001). A zebrafish histone variant H2A.F/Z and a transgenic H2A.F/Z:GFP fusion protein for in vivo studies of embryonic development. *Dev. Genes Evol.* **211**, 603-610.

Pontoriero, G. F., Smith, A. N., Miller, L.-A. D., Radice, G. L., West-Mays, J. A. and Lang, R. A. (2009). Co-operative roles for E-cadherin and N-cadherin during lens vesicle separation and lens epithelial cell survival. *Dev. Biol.* **326**, 403-417.

Shi, Y., De Maria, A., Lubura, S., Sikic, H. and Bassnett, S. (2015). The penny pusher: a cellular model of lens growth. *Invest. Ophthalmol. Vis. Sci.* **56**, 799-809.

Shimizu, T., Yabe, T., Muraoka, O., Yonemura, S., Aramaki, S., Hatta, K., Bae, Y.-K., Nojima, H. and Hibi, M. (2005). E-cadherin is required for gastrulation cell movements in zebrafish. *Mech. Dev.* **122**, 747-763.

Šikić, H., Shi, Y., Lubura, S. and Bassnett, S. (2015). A stochastic model of eye lens growth. *J. Theor. Biol.* **376**, 15-31.

Upadhya, D., Ogata, M. and Reneker, L. W. (2013). MAPK1 is required for establishing the pattern of cell proliferation and for cell survival during lens development. *Development* **140**, 1573-1582.

Urasaki, A., Morvan, G. and Kawakami, K. (2006). Functional dissection of the Tol2 transposable element identified the minimal cis-sequence and a highly repetitive sequence in the subterminal region essential for transposition. *Genetics* **174**, 639-649.

Westerfield, M. (1993). *The Zebrafish Book A Guide for the Laboratory Use of Zebrafish (Danio rerio)*. Portland, OR: The University of Oregon Press.

Xu, L., Overbeek, P. A. and Reneker, L. W. (2002). Systematic analysis of E-, N- and P-cadherin expression in mouse eye development. *Exp. Eye Res.* **74**, 753-760.

Yonemura, S., Wada, Y., Watanabe, T., Nagafuchi, A. and Shibata, M. (2010). alpha-Catenin as a tension transducer that induces adherens junction development. *Nat. Cell Biol.* **12**, 533-542.

Zhou, M., Leiberman, J., Xu, J. and Lavker, R. M. (2006). A hierarchy of proliferative cells exists in mouse lens epithelium: implications for lens maintenance. *Invest. Ophthalmol. Vis. Sci.* **47**, 2997-3003.

Supplementary figures

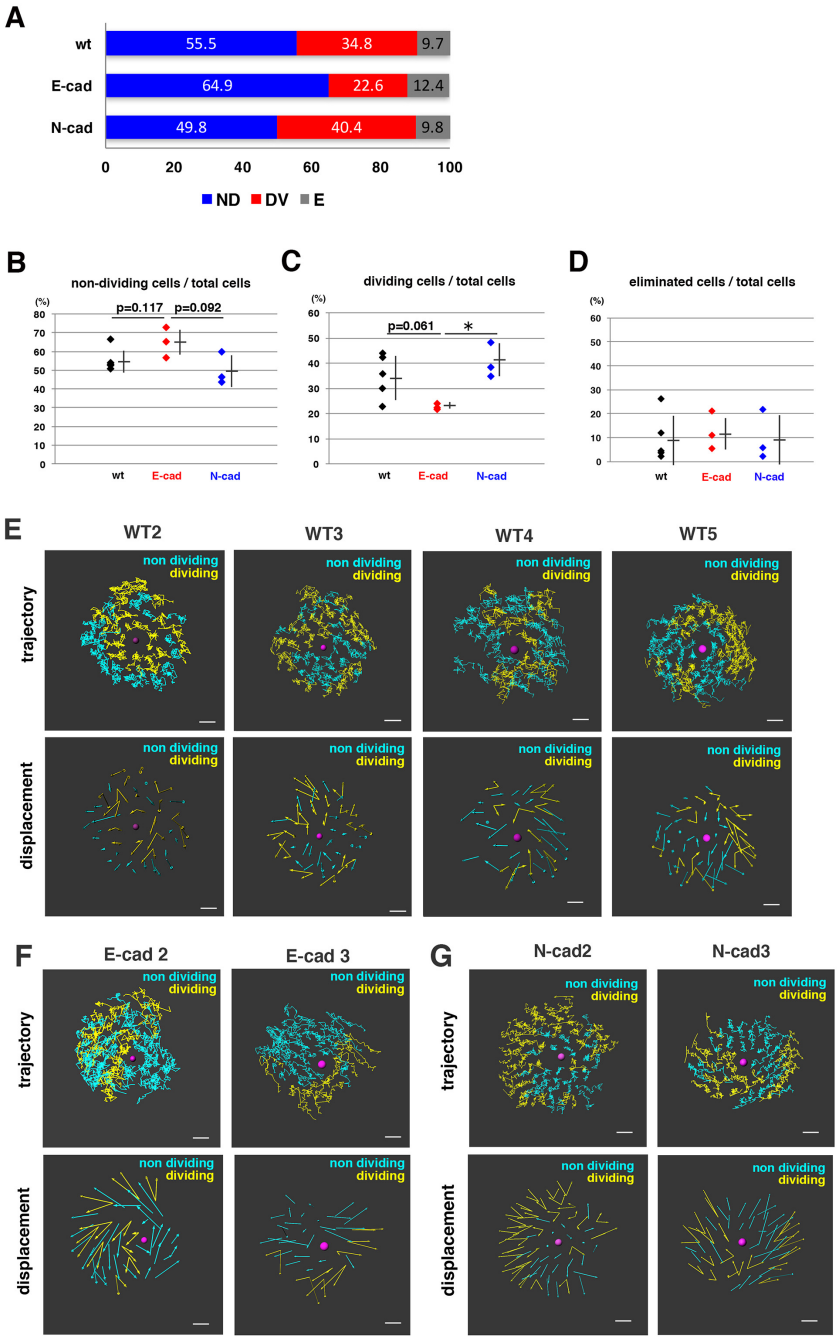

Figure S1. Fraction of non-dividing, dividing and eliminated cell populations in wild-type, E-cadherin mutant and N-cadherin morphant lenses

(A) Histogram of mean percentages of non-dividing (ND, blue), dividing (DV, red) and eliminated (E, grey) cell populations in five wild-type, three E-cadherin mutant, and three N-cadherin morphant lenses at 33 hpf. The fraction of dividing cell population was lower in E-cadherin mutant than in wild-type and N-cadherin morphant lenses.

(B–D) Fractions of non-dividing (B), dividing (C) and eliminated (D) cell populations in the anterior lens epithelium of the wild type, the E-cadherin mutant and the N-cadherin morphant at 33 hpf. Values for five wild-type, three E-cadherin mutant and three N-cadherin morphant lenses are plotted. Means and standard deviations are indicated by horizontal bars and vertical lines, respectively. Probabilities are calculated using Student's *t*-test: *p<0.05. In the case that probabilities are 0.05<p<0.15, p-values are indicated. The fraction of dividing cell population was lower in E-cadherin mutant than in wild-type and N-cadherin morphant lenses, although the difference between wild-type and E-cadherin mutant lenses was less significant (p=0.061 in (C)).

(E–G) Cell movement trajectory and displacement of additional four wild-type (E), two E-cadherin mutant (F), and two N-cadherin morphant lenses that we analyzed in this study. Scale bars: 10 μm.

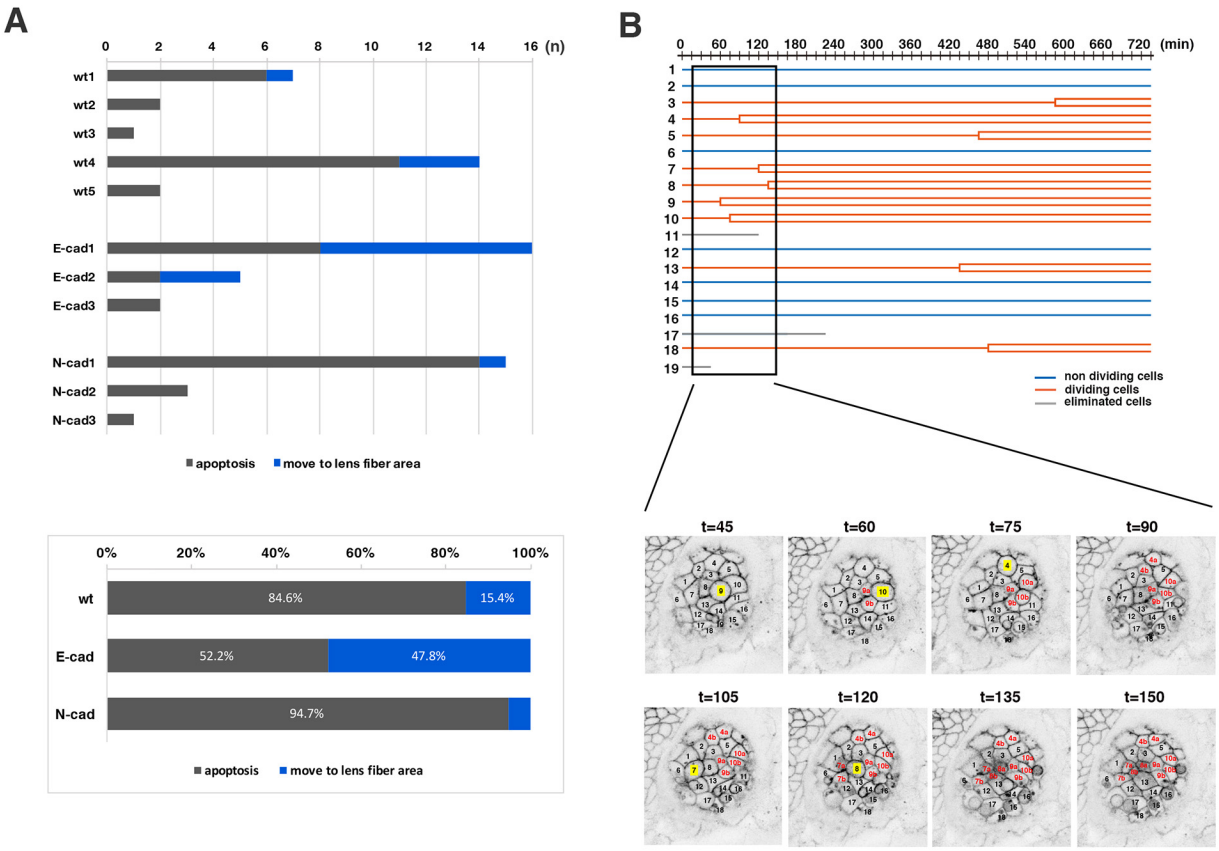

Figure S2. Analyses of the eliminated cell population and clustered cell divisions of wild-type lenses

(A) (Upper panel) Number of two types of eliminated cell population, which underwent apoptosis (grey) and moved into the lens fiber area (blue), respectively, in individual wild-type, E-cadherin mutant, and N-cadherin morphant lenses. The number of eliminated cells were varied depending on individual lenses. Eliminated cells that moved into the lens fiber area were generally observed in lenses with a high number of eliminated cells. (Lower panel) Histogram of the percentages of two types of eliminated cell population, which underwent apoptosis (grey) and moved into the lens fiber area (blue), respectively, relative to the total number of eliminated cells observed in five wild-type, three E-cadherin mutant, and three N-cadherin morphant lenses. The fraction of eliminated cells that moved into the lens fiber area was higher in E-cadherin mutant lenses (47.8%) than in wild-type lenses (15.4%), suggesting that E-cadherin suppresses cell movement from lens epithelium into the lens fiber area. In N-cadherin morphant lenses, this fraction was only 5.3%, much less than in wild-type lenses (15.4%).

(B) (Upper panel) Lineages of lens epithelial cells from zebrafish transgenic line, *Tg(h2afva:GFP; EF1α:mCherry-CAAX)* from 33 to 45 hpf, also shown in Movie2. Red, blue, and grey lines indicate dividing, non-dividing, and eliminated cell populations, respectively. (Lower panel) Confocal images for 135 min shown as squares in the upper panel. Only mCherry-CAAX fluorescence is shown. Numbers on individual cells correspond to cell numbers in the upper panel. Yellow squares and red numbers indicate mitotic cells and their daughter cells, respectively.

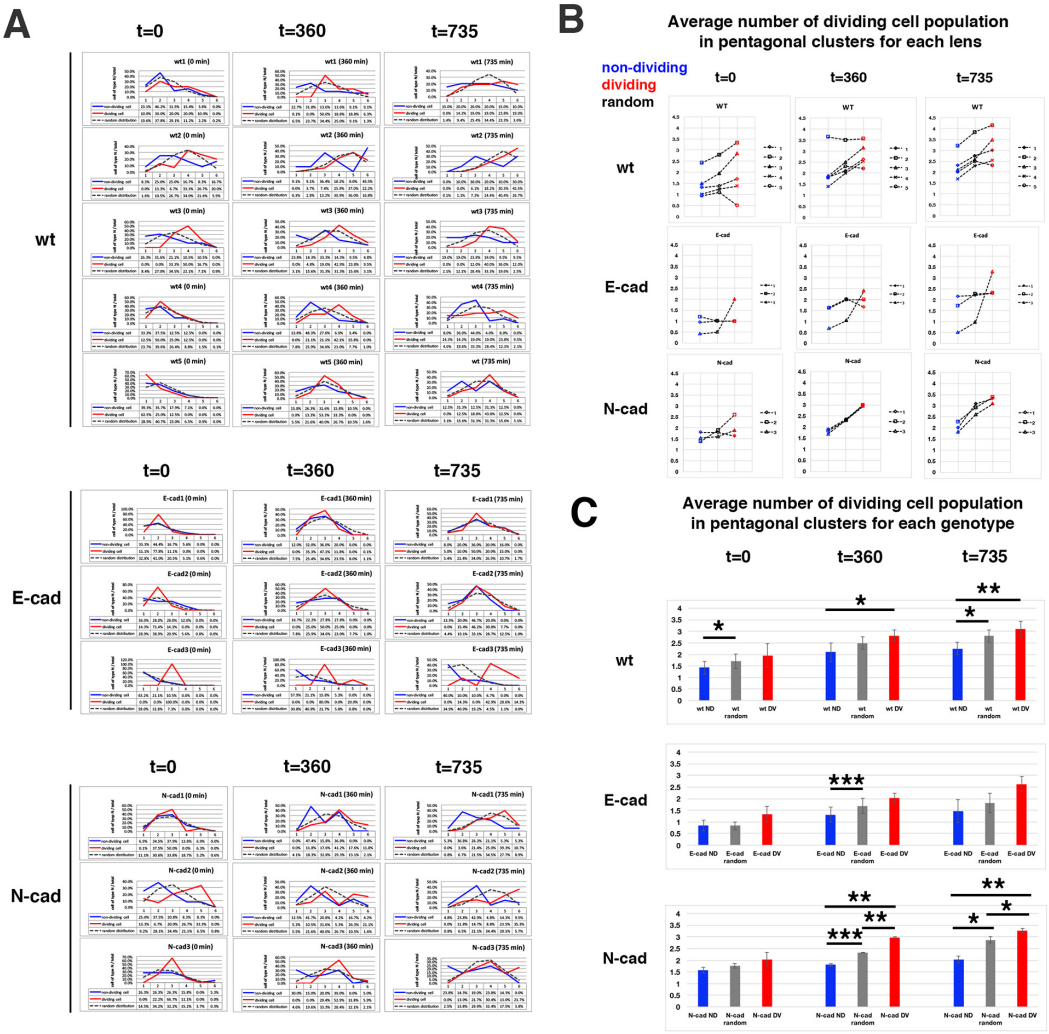

Figure S3. Analyses of non-dividing and dividing cell population clusters

(A) Distribution of pentagonal patterns of five wild-type, three E-cadherin mutant, and three N-cadherin morphant lenses during the scanned period. Times indicate the time elapsed after 33 hpf. Data at the end of the scanned period (t=735 min) are also shown in Figs. 1E, 3C, and 4C. Grey dotted lines indicate the profile of pentagonal patterns when non-dividing and dividing cell populations are randomly selected, whereas red and blue solid lines indicate the profiles of pentagonal patterns, in which cells pre-designated as dividing and non-dividing cell populations are in the center. Although distribution profiles were variable depending on individual lenses, distribution profiles of non-dividing and dividing cell population-centered pentagonal clusters were similar to that of random distribution model at t=0 in three of five wild-type lenses, two of three E-cadherin mutant lenses, and two of three N-cadherin morphant lenses. Non-dividing and dividing cell populations were gradually segregated to form clusters during development in wild-type and N-cadherin morphant lens epithelium. However, such segregation did not occur in lens epithelium of two E-cadherin mutant lenses, E-cad1 and E-cad2, during the scanned period. In one E-cadherin mutant lens, E-cad3, the distribution profile of dividing cell population-centered pentagonal clusters was strongly segregated from that of the random distribution model even at t=0, probably because dividing cells were extremely localized in the peripheral region (see Fig. S1F).

(B) Average number of dividing cell population in pentagonal clusters of each of wild-type, E-cadherin mutant and N-cadherin morphant lenses. In wild-type and N-cadherin morphant lenses, values of dividing and non-dividing cell population-centered pentagonal clusters gradually became higher and lower than those of random distribution model, respectively during the scanned period. However, in E-cadherin mutant lenses, two lenses showed similar numbers of non-dividing and dividing cell population-centered pentagonal clusters compared to the random distribution model at t=360 and 735, suggesting that segregation of non-dividing and dividing cell populations does not proceed normally in E-cadherin mutant lenses.

(C) Average number of dividing cell population in pentagonal clusters of five wild-type, three E-cadherin mutant, and three N-cadherin morphant lenses. Bar indicates standard error. Student's *t*-test: *p<0.05, **p<0.01, ***p<0.001. Significant differences between non-dividing cell population-centered clusters and dividing cell population-centered clusters were observed in wild-type and N-cadherin morphant lenses at 360 and 735 min. Furthermore, segregation between random distribution and non-dividing/dividing cell populations-centered clusters was enhanced in N-cadherin morphant lenses. On the other hand, there were no significant difference between non-dividing cell population-centered clusters and dividing cell population-centered clusters in E-cadherin mutant lenses.

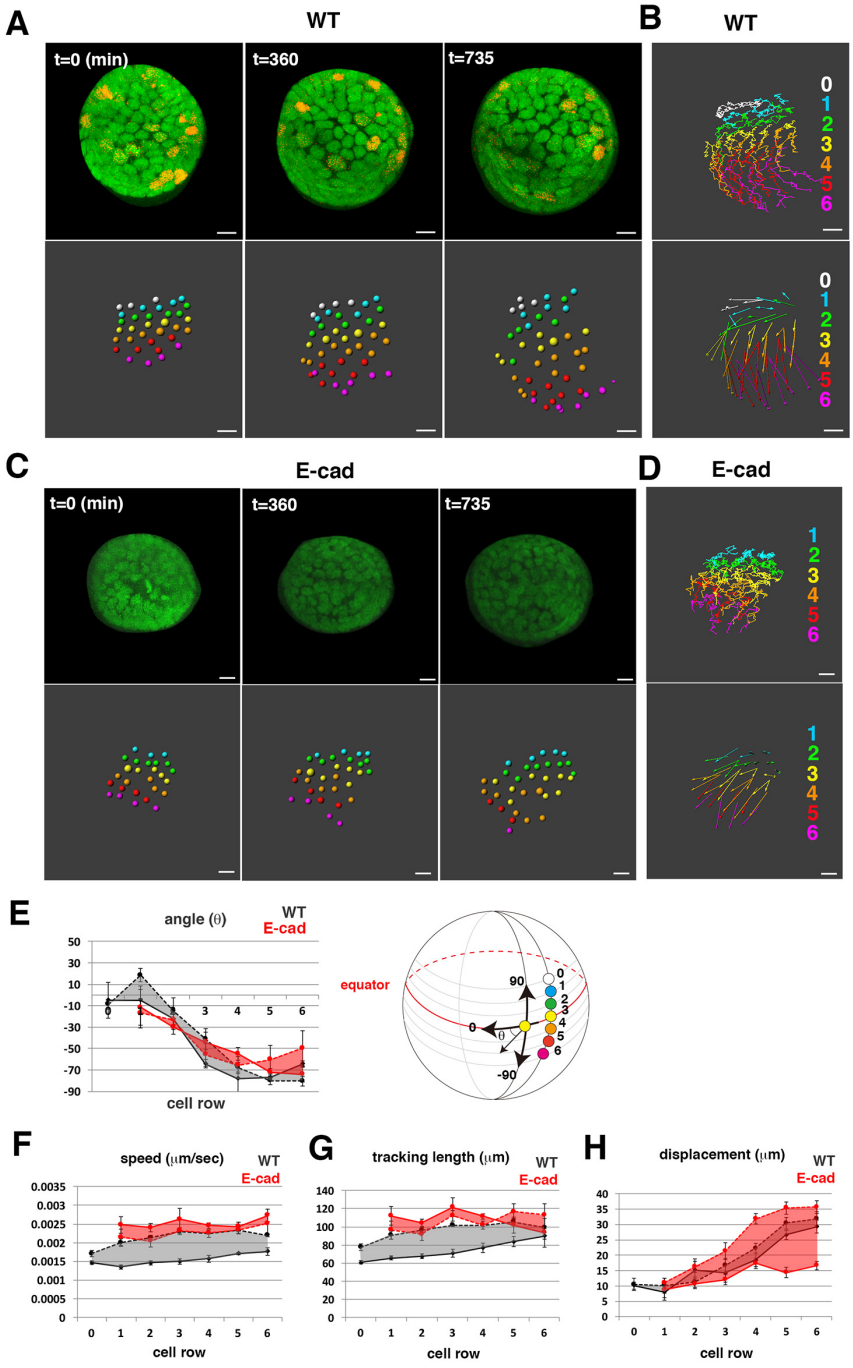

Figure S4. Cell movement in the equatorial region of the wild-type and the E-cadherin mutant

(A, C) Confocal images (upper) and nuclear positions (lower) in the equatorial region of wild-type (A) and *hab*^{rk3} mutant (C) lenses combined with *Tg(h2afva:GFP; EF1α:mCherry-zGem)*. Times elapsed after 33 hpf are indicated.

(B, D) Trajectory (upper) and displacement (lower) of cell movement in the equatorial region of wild-type (B) and *hab*^{rk3} mutant (D) lenses.

(E) Cell movement direction in the equatorial region of two wild-type (black) and *hab*^{rk3} mutant (red) lenses. Solid lines indicate the lens shown in (A–D). The zone between two lenses is indicated in color. The right panel indicates the definition of cell movement direction (θ).

(F–H) Speed (F), tracking length (G) and displacement (H) of cell movement in the equatorial region of two wild-type (black) and *hab*^{rk3} mutant (red) lenses. Solid lines indicate the lens shown in (A–D). The zone between two lenses is indicated in color.

Error bars indicate the standard error of the mean. Scale: 10 μm (A-D).

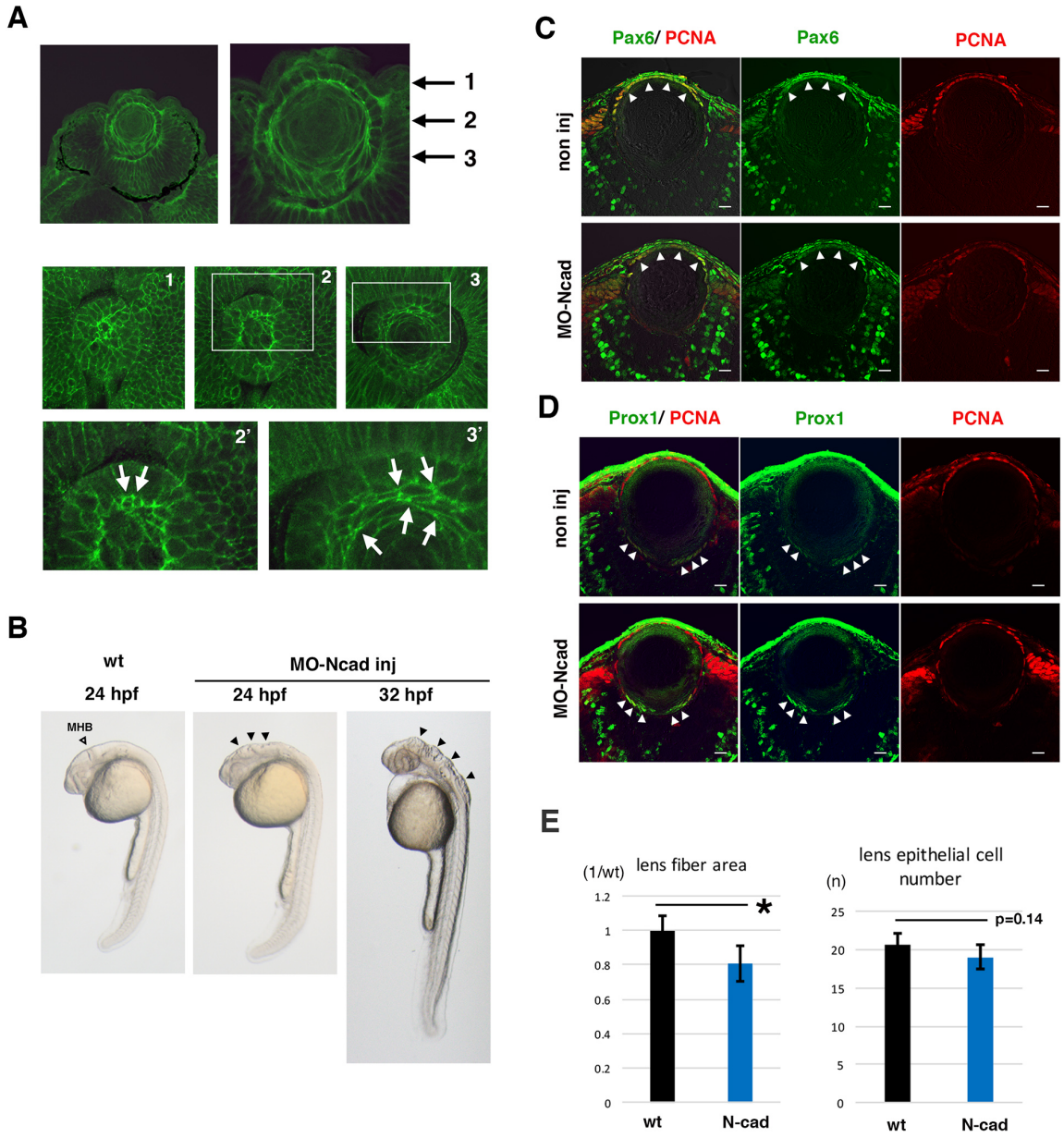

Figure S5. Lens fiber growth defects in an N-cadherin morphant

(A) Immuno-labeling of zebrafish lens with anti-N-cadherin antibody. The top two panels show sections of the retina and lens at 33 hpf. The middle three and bottom two panels show confocal scanning of horizontal planes in whole mount lens at 27 hpf. Three planes perpendicular to the AP axis, which contain the apical lens fiber suture (plane 1), the equatorial area (plane 2), and elongating lens fiber cells (plane 3), are shown in panels 1, 2, and 3, respectively. The bottom two panels indicate higher magnification images of white squares shown in panels 2 and 3. N-cadherin protein is markedly accumulated in plasma membrane of apical tips (arrows in panel 2') and the intermediate flattened region (arrows in panel 3') of lens fiber cells. These data suggest that N-cadherin is strongly expressed in elongating lens fiber cells.

(B) Morphology of N-cadherin morphant embryos at 24 and 32 hpf. The open arrowhead indicates the position of the midbrain-hindbrain boundary (MHB) in wild-type 24 hpf embryos. Black arrowheads indicate the failure of neural tube closure around the MHB in N-cadherin morphant embryos at 24 and 32 hpf.

(C–D) Labeling of wild-type and N-cadherin morphant lenses with antibodies against PCNA (red, C and D), Pax6 (green, C) and Prox1 (green, D). In the N-cadherin morphant, lens epithelial cells and differentiating lens fiber cells normally express Pax6 (arrowheads, C) and Prox1 (arrowheads, D), respectively.

(E) Histogram of lens fiber area size (left) and the number of lens epithelial cells (right) in wild-type (black) and N-cadherin morphants (blue). Six independent lenses for 72 hpf wild-type and N-cadherin morphant embryos were used to measure lens fiber area size with Image-J and to count lens epithelial cells on plastic sections that cover the central region of the lens sphere. The standard deviation is indicated. Student's *t*-test; * $p<0.05$. Scale: 10 μm (C, D).

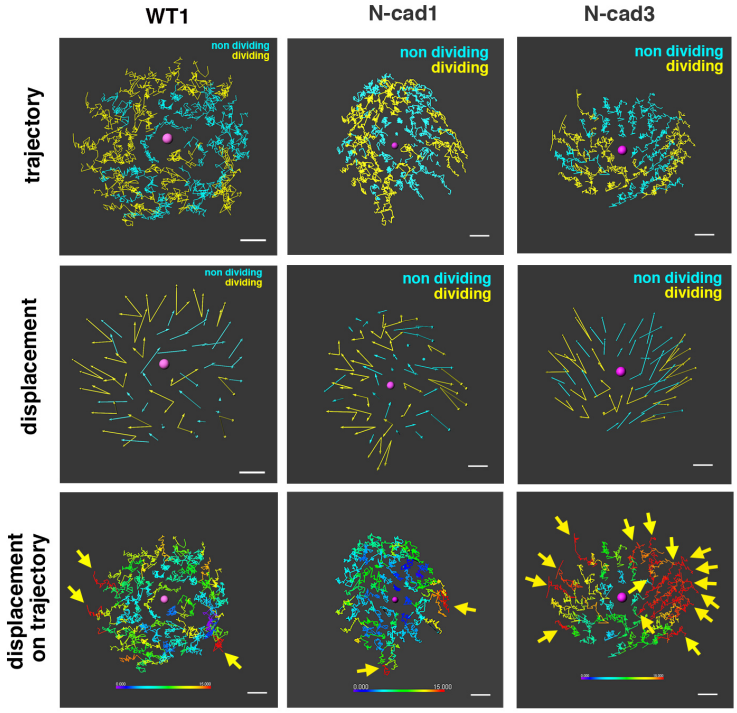

Figure S6. Analyses of cell movement in the anterior lens epithelium of an N-cadherin morphant
Trajectory (upper panels) and displacement (middle panels) of lens epithelial cells in wild-type, namely WT1, and N-cadherin morphant lenses, namely N-cad1 and N-cad3. The N-cad1 lens above is also shown in Figure 3. Blue and yellow colors indicate non-dividing and dividing cell populations, respectively. In the N-cad3 lens, the dividing cell population was unevenly located in the anterior epithelium. (Bottom panels) Displacement length shown in the trajectory of lens epithelial cells. The color range from blue to red corresponds to displacement length from low (0 μm) to high (15 μm), respectively. WT1, N-cad1, and N-cad3 lenses are shown. Yellow arrows indicate cells with longer displacements (>15 μm, red). The WT1 and N-cad1 lenses have a few long-displacement cells only in the peripheral region, whereas the N-cad3 lens has 15 long-displacement cells. Scale: 10 μm.

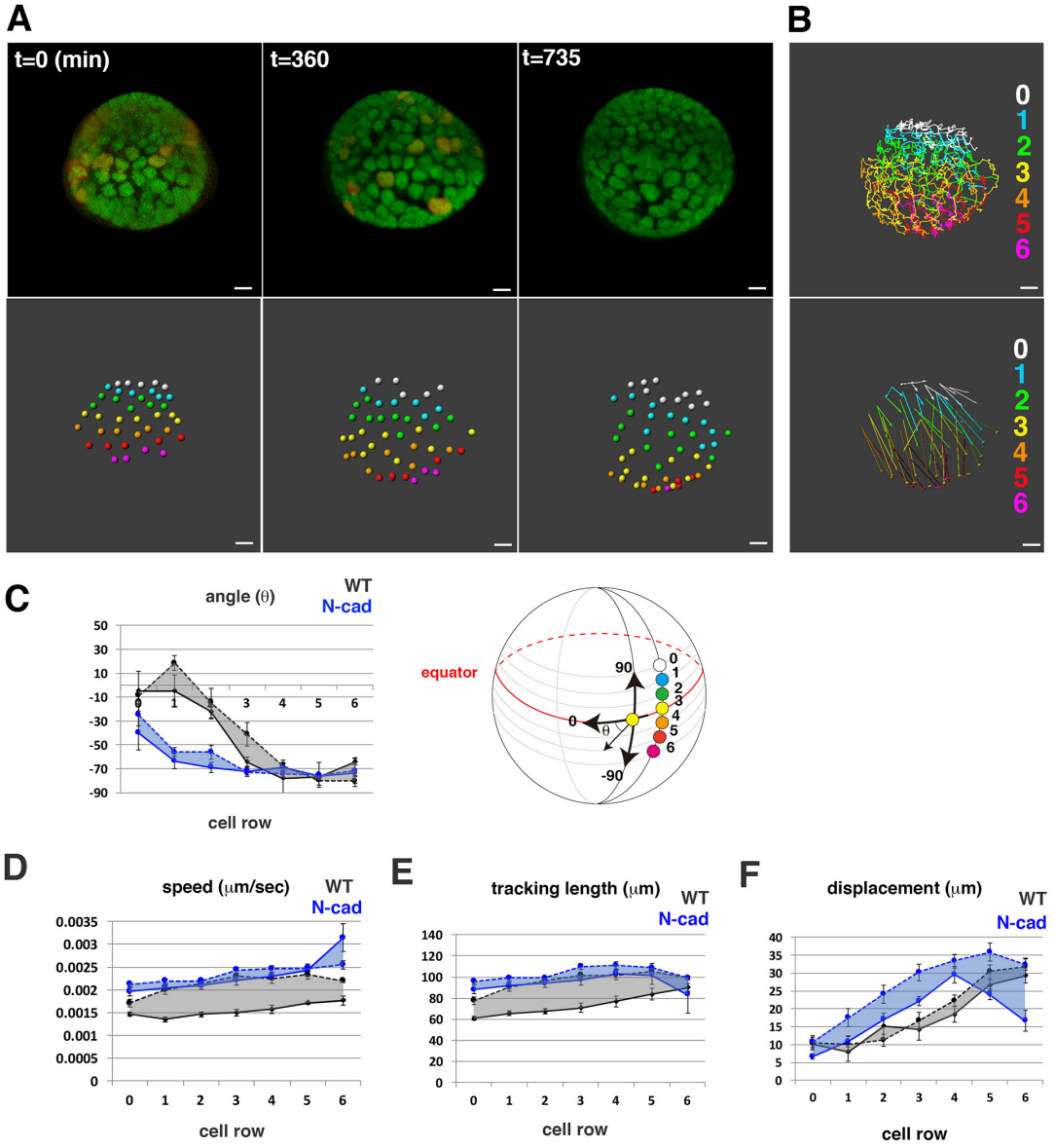

Figure S7. Cell movement in the equatorial region of an N-cadherin morphant

(A) Confocal images (upper) and nuclear positions (lower) of the equatorial region of an N-cadherin morphant lens combined with *Tg(h2afva:GFP; EF1α:mCherry-zGem)*. Time elapsed after 33 hpf is indicated.

(B) Trajectory of cell movement (upper) and cell displacement (lower) in the equatorial region of an N-cadherin morphant.

(C) Cell movement direction in the equatorial region of two wild-type (black) and N-cadherin morphant (blue) lenses. Solid lines indicate the lens shown in (A–B). The zone between two lenses is colored.

(D–F) Speed (D), tracking length (E) and displacement (F) in the equatorial region of two wild type (black) and N-cadherin morphant (blue) lenses. Solid lines indicate the lens shown in (A–B). The zone between two lenses is indicated in color. Error bars indicate the standard error of the mean. Scale: 10 μm (A–B).

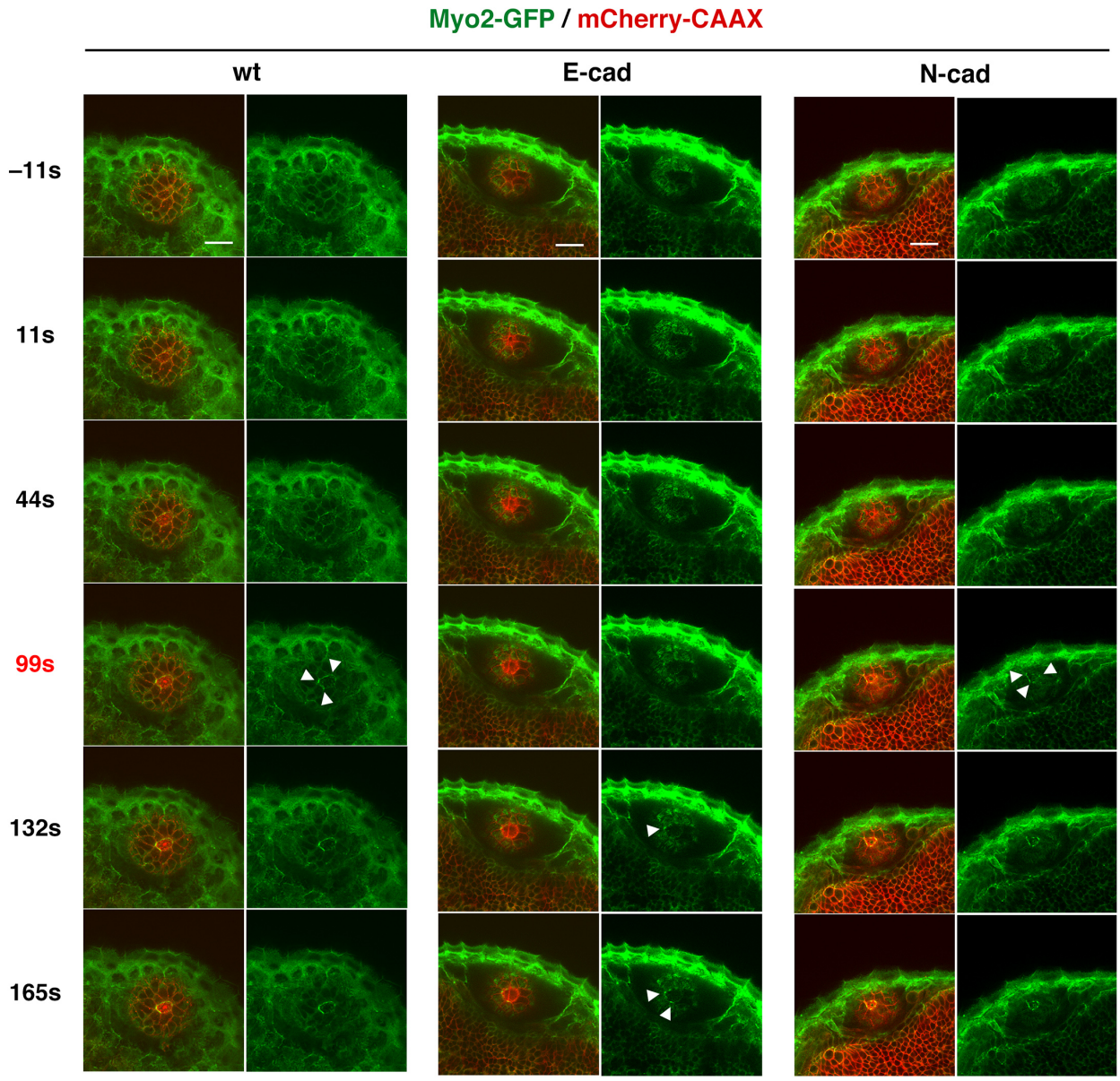

Figure S8. Analyses of Myosin2 accumulation in response to laser ablation
Time-lapse scanning of 50 hpf wild-type, E-cadherin, and N-cadherin morphant lens epithelia expressing *Tg(actb1:myl12.1-eGFP; EF1α: mCherry-CAAX)* after laser ablation. The right columns indicate only the green channel (Myosin 2). White arrowheads indicate accumulation of Myosin2 in cell membranes surrounding the ablated area. Myosin2 accumulated in all cases: wild-type, E-cadherin and N-cadherin morphant lenses, although accumulation was delayed in E-cadherin morphant lenses and occurred irregularly in patches in both E- and N-cadherin morphant lenses. Scale: 20 μm.

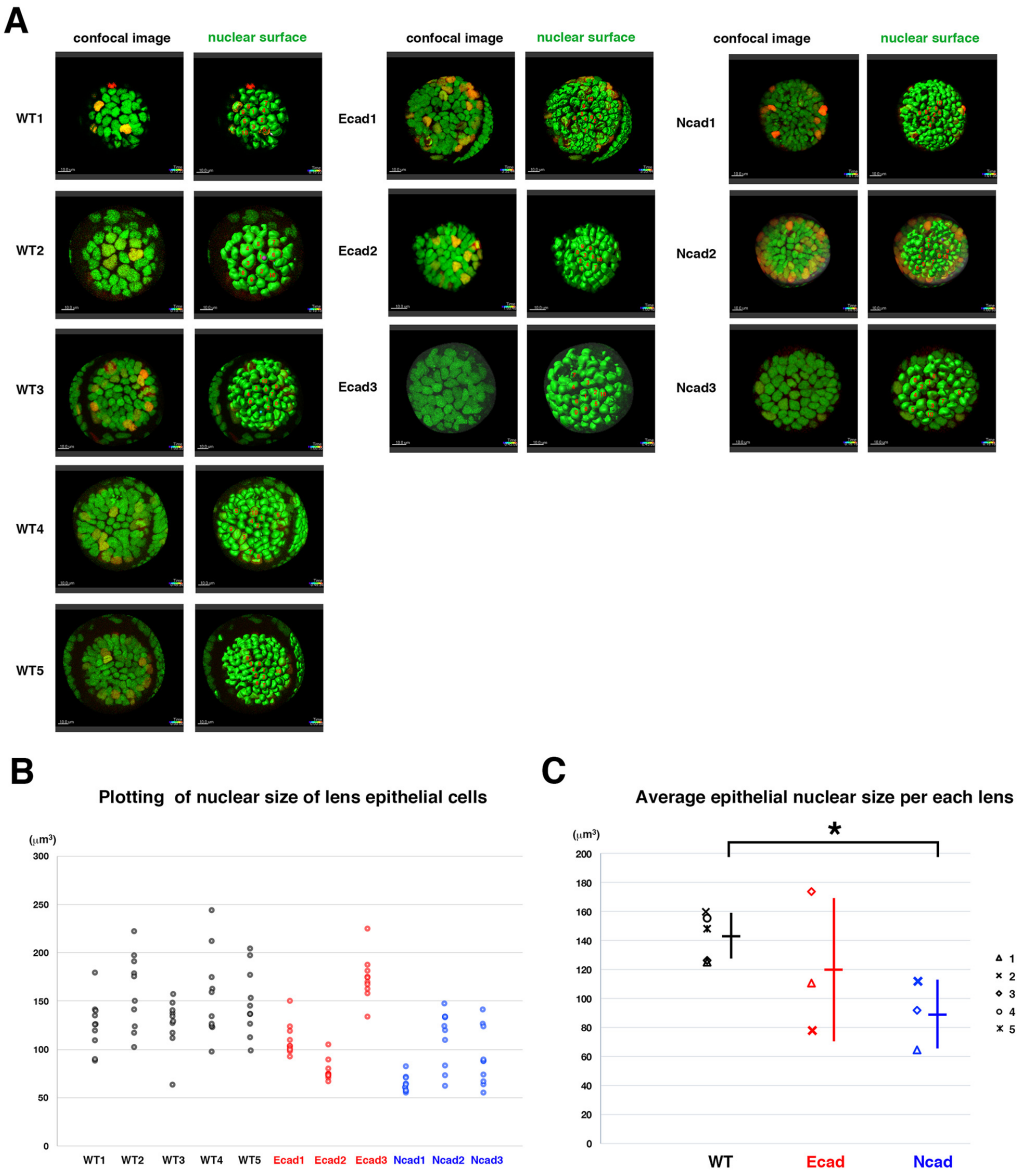

Figure S9. Analyses of nuclear size of lens epithelial cells

(A) Confocal images (left) and surface objects demarcating lens epithelial nucleus (right) in wild-type, E-cadherin mutant, and N-cadherin morphant anterior lens epithelia at an early stage of the scanned period: 33–36 hpf. Ten lens epithelial cell nuclei randomly selected for measurement of nuclear volume are indicated in red in the right panels.

(B) Plotting of nuclear volumes of individual lens epithelial cells per each of wild-type, E-cadherin mutant, and N-cadherin morphant lenses. Distribution range was variable depending on individual lenses, but the range was reduced in E-cad1, E-cad2 and three N-cad lenses and elevated in E-cad3 lenses, compared with wild-type lenses.

(C) Plotting of average nuclear volumes of lens epithelial cells in each lens. Horizontal bars and vertical lines indicate mean and standard deviation of lens epithelial nuclear volume, respectively. Nuclear size of lens epithelial cells was significantly smaller in the N-cadherin morphant than in wild type, whereas the range was broader in the E-cadherin mutant than in wild type. In the N-cadherin morphant, a reduced tensile force and prominent E-cadherin-dependent cell adhesion may reduce nuclear size. In E-cadherin mutant, the absence of adherens junction may weaken the tensile force transmission from plasma membranes to nuclear membranes, resulting in variable nuclear size. Probability is calculated using Student's *t*-text: *p<0.05.

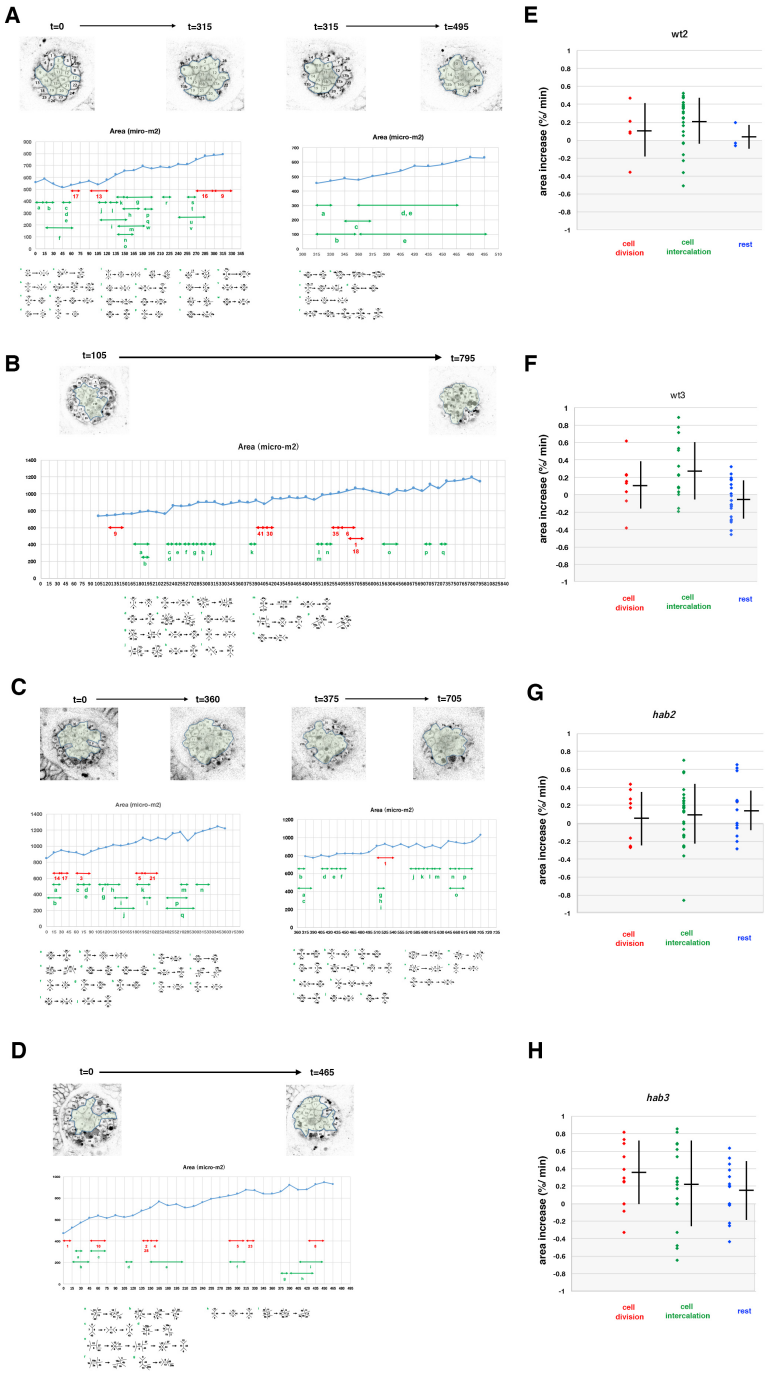

Figure S10. Analyses of lens epithelial expansion of wild-type and E-cadherin mutant lenses

(A, B) Lens epithelial expansion analysis of two wild-type lenses, namely wt2 (A) and wt3 (B). The top panels indicate the composition of individual lens epithelial cells. Middle panels display temporal profiles of the area. Red and green arrows indicate cell division events and periods when cell intercalation occurred, respectively. Bottom panels indicate cell intercalation that occurred in the corresponding period of middle panels.

(C, D) Lens epithelial expansion analysis of two *hab*^{rk3} mutant, namely *hab2* (C) and *hab3* (D).

(E, F) Plotting of expansion rate per each scanned frame (15 min) of two wild-type (A, B) lens epithelial areas during periods of cell division (red), cell intercalation (green), and the rest period without cell division or intercalation (blue). Horizontal bars and vertical lines indicate the mean and standard deviation, respectively.

(G, H) Plotting of expansion rate per each scanned frame (15 min) of two *hab*^{rk3} mutant (C, D) lens epithelial areas during periods of cell division (red), cell intercalation (green), and the rest period without cell division or intercalation (blue). Horizontal bars and vertical lines indicate the mean and standard deviation, respectively.

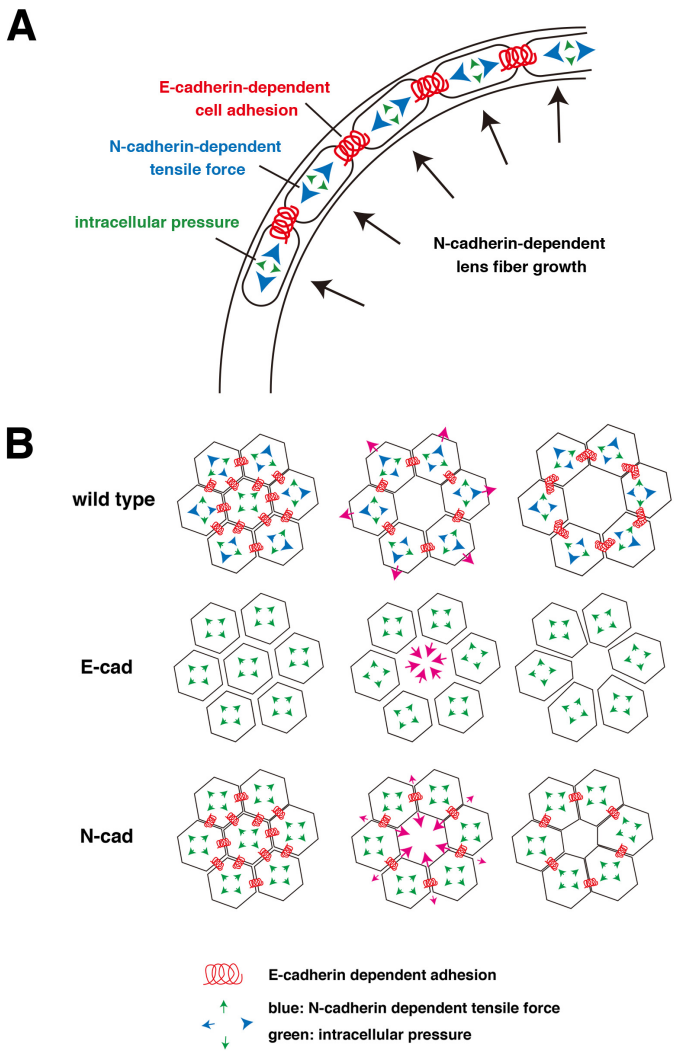

Figure S11. A possible model of lens epithelial forces

(A) N-cadherin promotes lens fiber growth, which increases epithelial tension (blue arrowheads). Force derived from intracellular pressure (green arrowheads) also contributes to the epithelial tension. E-cadherin, a component of adherens junctions (red springs), cooperates with the actomyosin-dependent shrinking force, and counterbalances these tensile forces between epithelial cells.

(B) (Left column) In the wild type, the E-cadherin-mediated cell adhesion force (red springs) counterbalances both the N-cadherin-mediated tensile force (blue arrowheads) and intracellular pressure (green arrowheads) to preserve epithelial tension as elastic energy in the lens epithelium. (Middle column) Removal of a single cell by laser ablation suddenly eliminates the E-cadherin-mediated cell adhesion force between the ablated cell and surrounding cells, resulting in predominance of the tensile force that pulls surrounding cells toward the outside. (Right column) This predominant pulling force induces recoil expansion of the ablated area just after laser ablation. After ~100 second-post ablation, an actomyosin-dependent healing process starts to close the ablated space.

In the E-cadherin mutant, the N-cadherin-mediated tensile force on the lens epithelium is intact. However, since adherens junctions are not absent in the E-cadherin mutant, lens epithelial cells do not sense the N-cadherin-mediated tensile force from neighboring cells. The absence of cell adhesion also increases fluidity of cell movement and flexibility of cell shape in the E-cadherin mutant. After laser ablation, E-cadherin mutant surrounding cells do not expand but passively start to close the ablated space. Since the actomyosin-dependent healing process depends on E-cadherin, the ablated space fails to be closed in the E-cadherin mutant in the later stage. Increased fluidity of cell shape may enlarge the apical size of E-cadherin mutant lens epithelial cells. It is also possible that the reduction of cell division decreases the size of the lens fiber core, which also contributes to reduction of epithelial tension in the E-cadherin mutant.

In the N-cadherin morphant, the N-cadherin-mediated tensile force on the lens epithelium is reduced. The E-cadherin-dependent cell adhesion force counterbalances only the intracellular pressure, which is likely to be less than the normal level of N-cadherin-mediated tensile force in wild type cells. This physical situation weakens the pulling tension preserved in the lens epithelium and shrinks the apical cell size. After laser ablation, surrounding cells do not expand but the ablated area started to close because of the predominant E-cadherin-mediated cell adhesion force between lens epithelial cells.

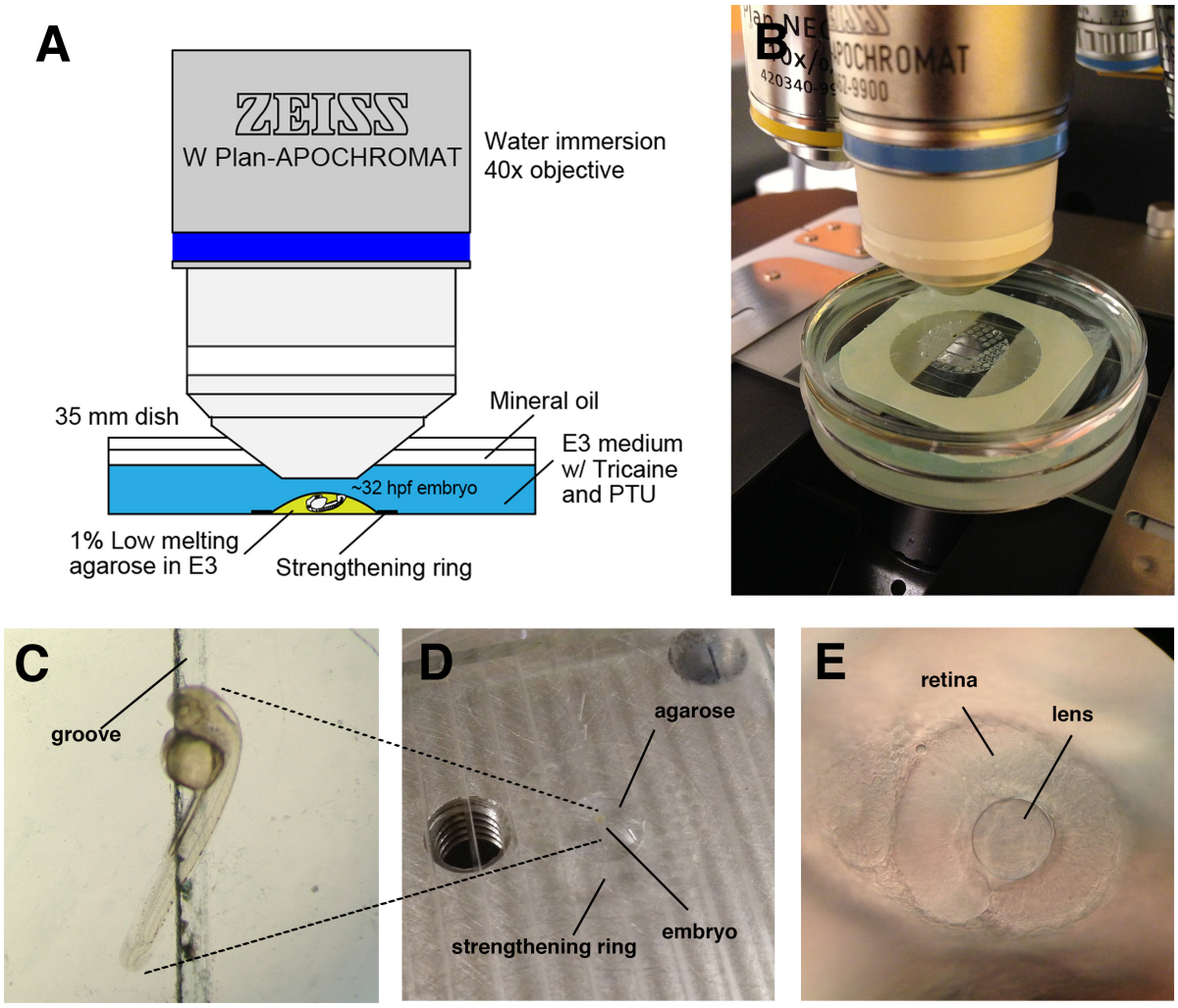

Figure S12. Set-up for time-lapse imaging of zebrafish lens epithelium

(A) Schematic illustration of the imaging setup.

(B) Real set-up picture.

(C) The embryo was mounted in 1% low-melting agarose, and the yolk was put into the groove in order to orient the embryo laterally.

(D) The agarose was restricted within the inner circle of a strengthening ring on the groove stretched into the acrylic plate.

(E) The lateral side of the embryonic eye was used for confocal z-stack scanning.

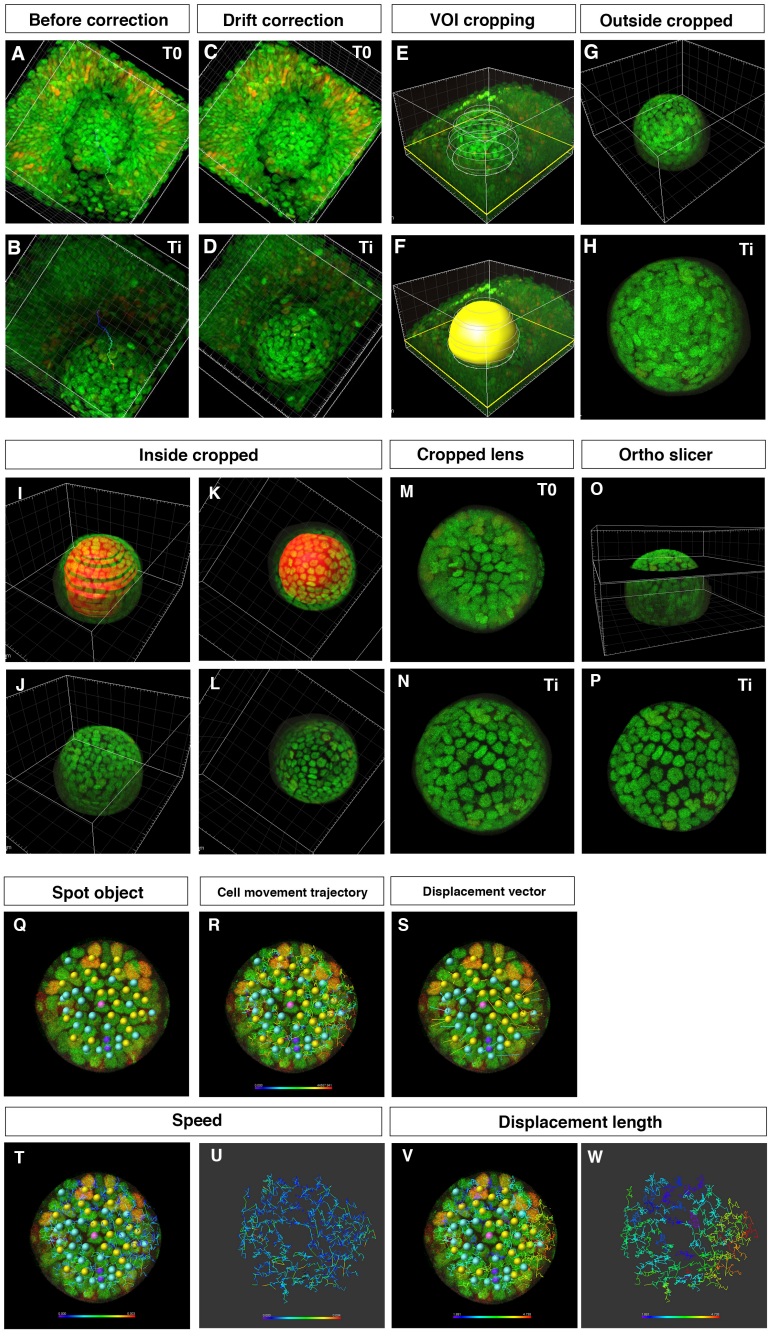

Figure S13. Procedure for obtaining 3D time-lapse images of anterior lens epithelium
(A–D) Two time points from T0 to Ti of embryonic eyes without (A, B) and with drift correction (C, D). (E, F) VOI cropping by drawing outside contour circles and creation of a surface masking the lens. (G, H) Outside cropped lens. (I–L) Cropping of the lens fiber area by drawing inside contour circles and by creating a surface masking the lens fiber area. (M, N) Cropped lens at T0 and Ti. (O, P) Extract of anterior lens epithelium using the "Ortho Slicer" tool. (Q–W) Analysis of cell movement of lens epithelial cells. (Q) Assignment of spot objects to trace cell lineages, which classify epithelial cells into dividing (yellow), non-dividing (blue), and eliminated cell populations (purple). (R) Cell movement trajectory, (S) displacement vector, (T–U) cell movement speed, and (V–W) displacement length.

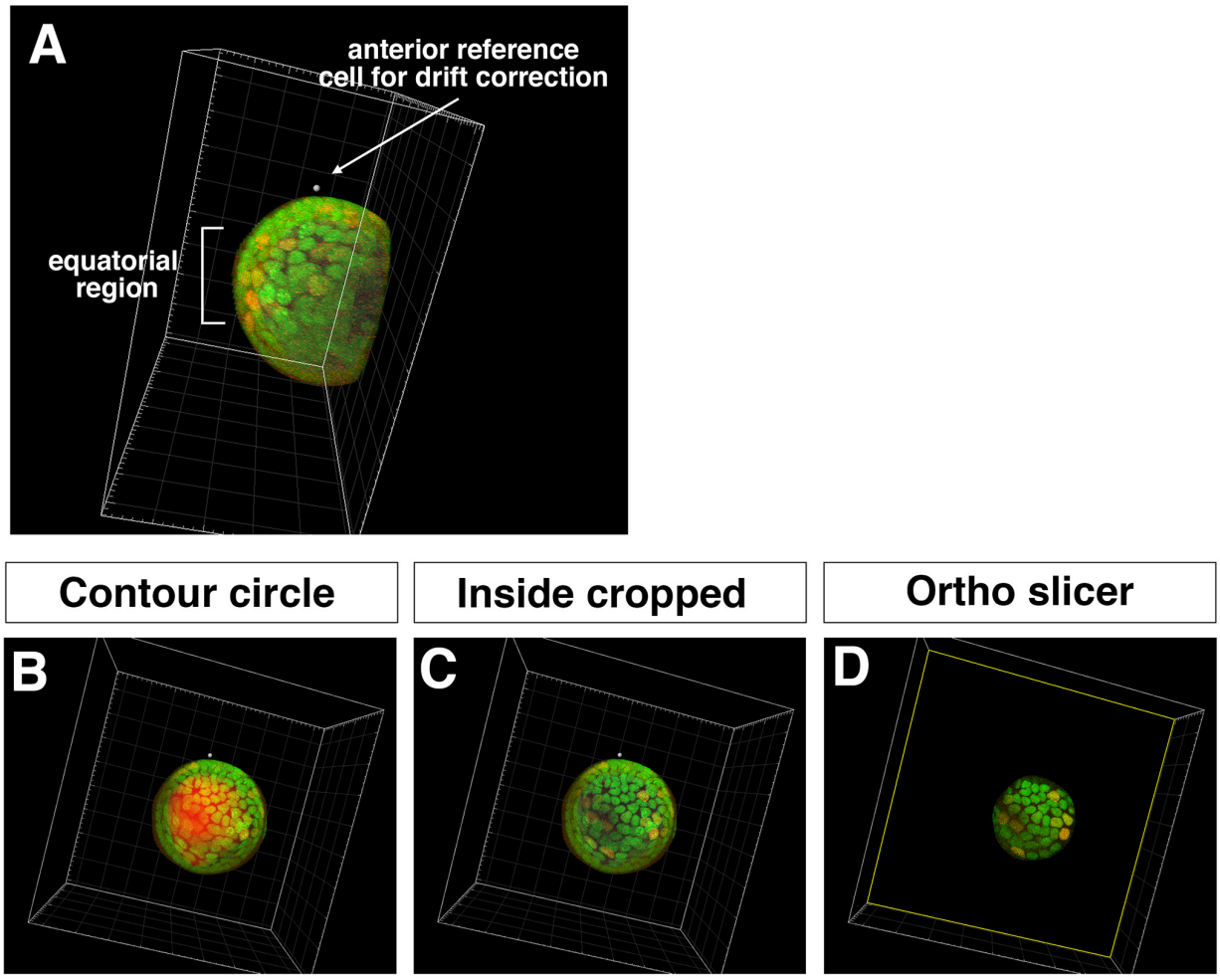

Figure S14. Procedure for obtaining 3D time-lapse images of equatorial lens epithelium

(A) Side view of the lens scanned from the ventral view. Tissues outside the lens sphere, such as the retina and the cornea, were removed by cropping. Anterior reference position used for drift correction and the equatorial region are indicated.

(B) Equatorial view of the lens before cropping the lens fiber core. Contour of the surface masking the lens fiber core is indicated (red).

(C) Equatorial view of the lens after cropping the lens fiber core.

(D) Only the equatorial lens epithelium was extracted using the "Ortho slicer" tool.

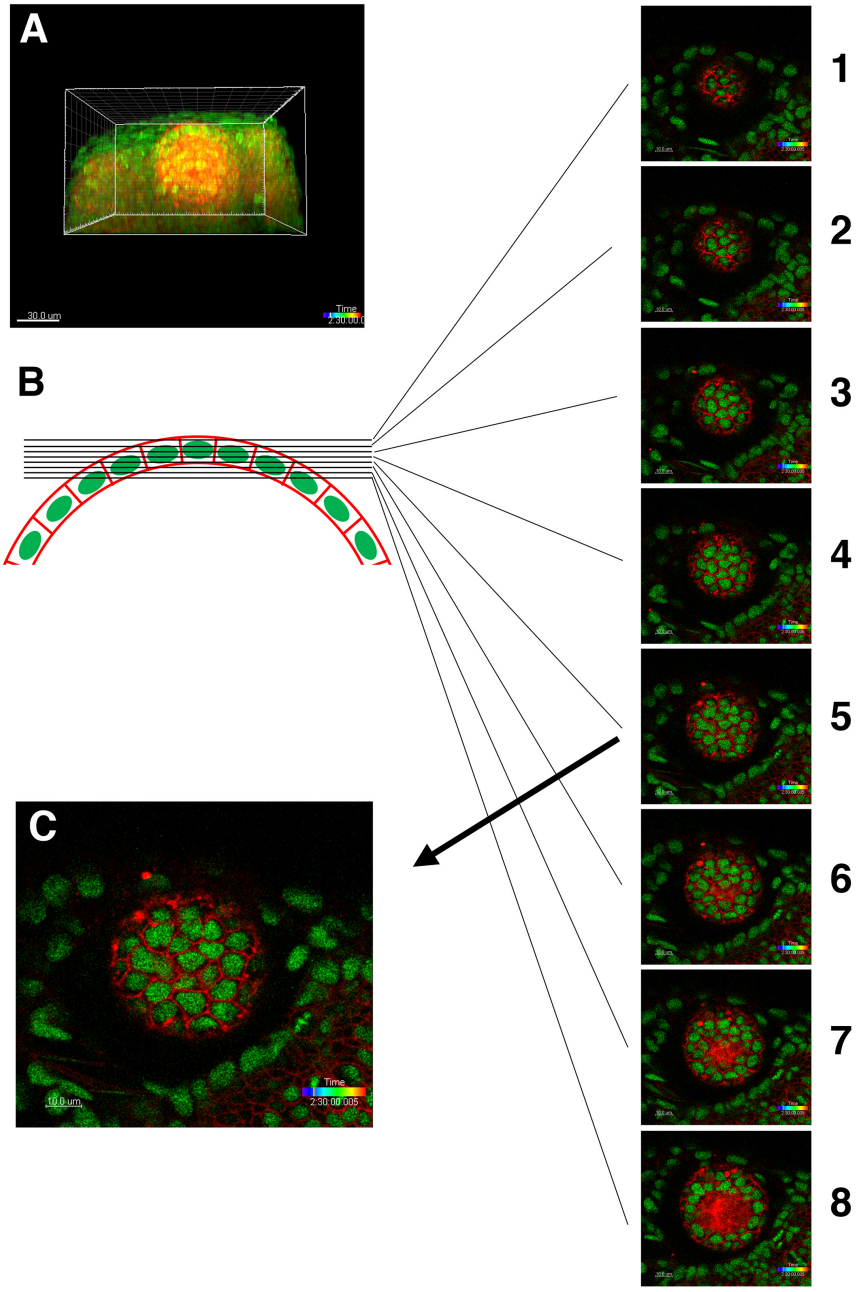

Figure S15. Procedure for selecting a confocal slice of the most apical lens epithelium

(A) 3D confocal image of *Tg(h2afva:GFP; EF1α:mCherry-CAAX)* transgenic fish lens.

(B) Schematic picture of zebrafish lens epithelium and z-axis slice level. Eight slices containing the anterior lens epithelium from the anterior to posterior direction are shown. The interval between neighboring slices is 1 μm. Three posterior slices, #6–8, contains the lens fiber region. Thus, the #5 slice is the most suitable for analysis of cell intercalation and epithelial rearrangement, because CAAX-labeled plasma-membranes correspond to the adherens junction complex-containing domain.

(C) The confocal slice containing the most apical lens epithelium just adjacent to the lens fiber core (indicated as the #5 slice in B), which was used to make a movie and to analyze cell division, cell intercalation, and area expansion.

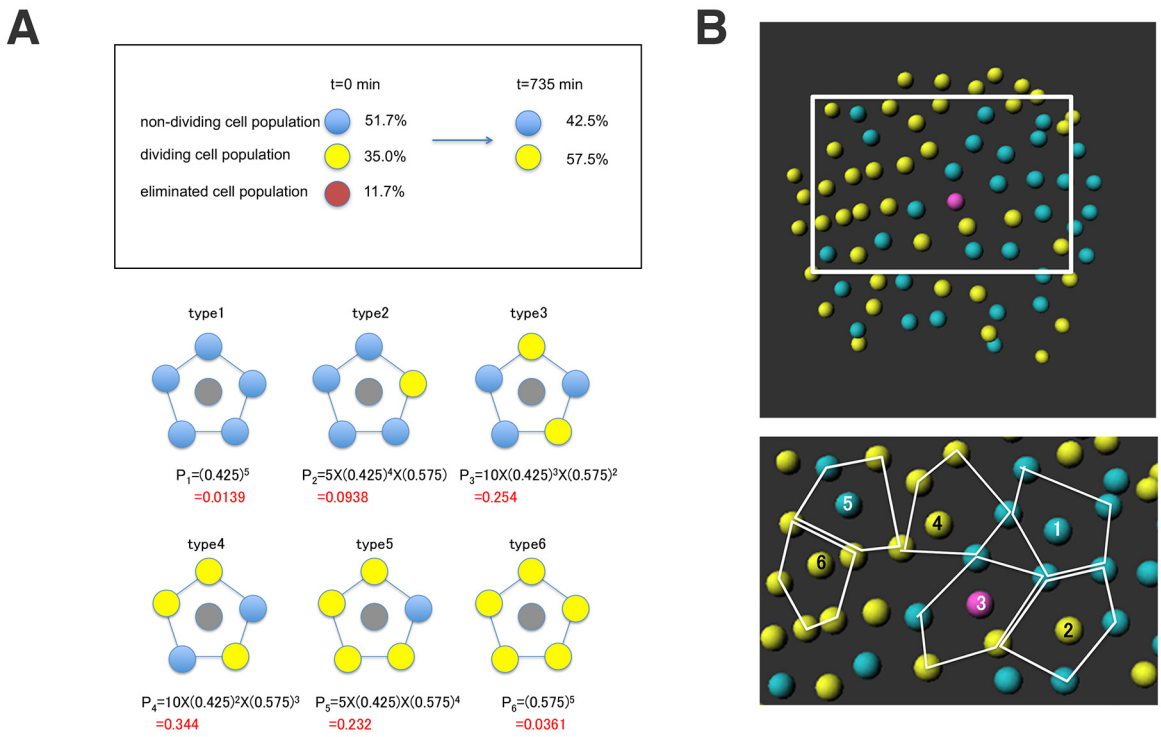

Figure S16. Analyses of non-dividing and dividing cell clusters

(A) Calculation of probability for each pentagonal pattern generated by the random distribution model. In the wild-type lens shown in Figure 1B, non-dividing (blue), dividing (yellow), and eliminated (red) cells comprise 51.7, 35.0, and 11.7% of all cells, respectively, at the beginning of the scanned period (33 hpf). At the end of scanned period (45 hpf), the final ratio of non-dividing and dividing cells is calculated as 42.5 and 57.5%, respectively. Bottom panels indicate six pentagonal patterns depending on combinations of non-dividing (blue) and dividing (yellow) cell populations. On the assumption that non-dividing and dividing cells are distributed at random, the probability for each pattern at 45 hpf is calculated by the equation below.

(B) Example of pentagonal patterns of wild-type lenses shown in Fig. 1B. The number indicates the type of pentagonal pattern.

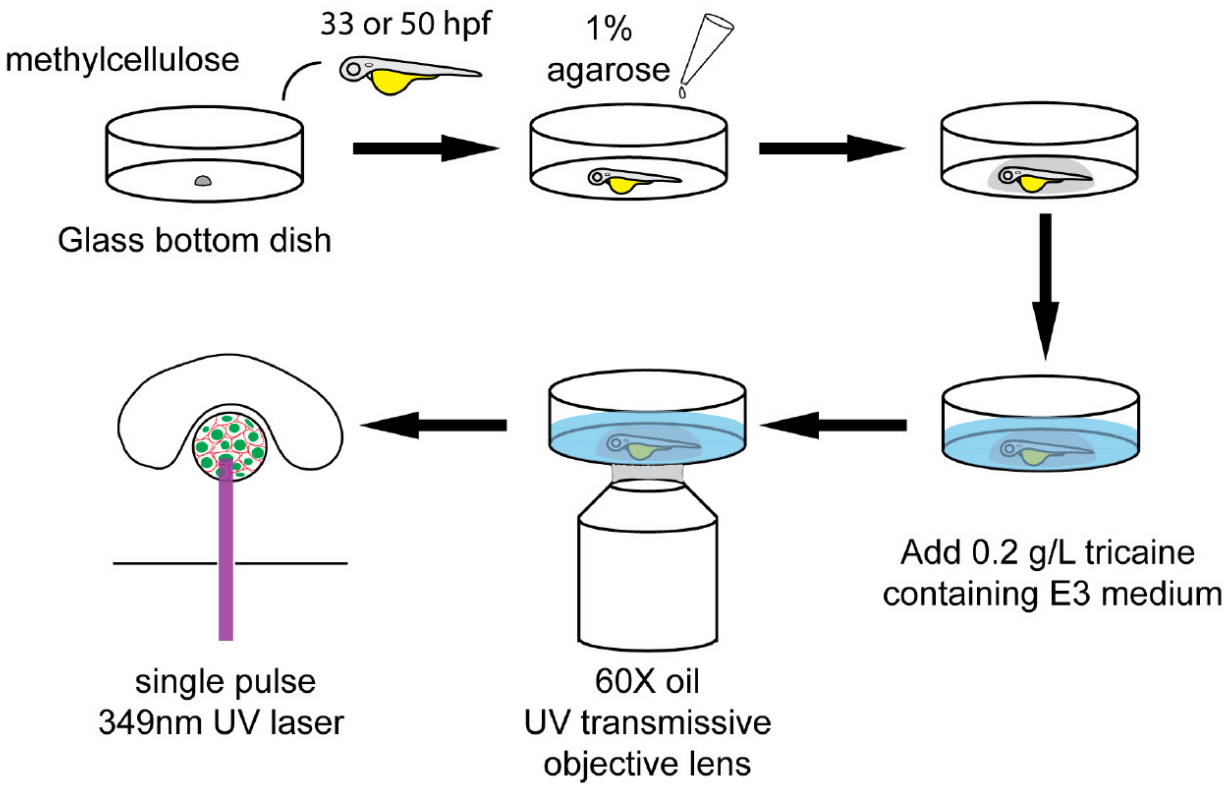

Figure S17. Procedure for mounting zebrafish embryos for laser ablation experiments
Fifty hpf embryos were mounted onto glass-bottom dishes with a drop of 3% methylcellulose, and oriented so that the eye was close to the bottom. Low-melting agarose buffered with E3 medium was then added on top of the embryos to hold the embryo orientation. After solidification of the agarose, E3 medium containing Tricaine was added just before UV laser ablation. After mounting of the dish containing an embryo on the stage of inverted confocal LSM microscope with 60x objective lenses, a single shot of 349nm-UV laser was fired to ablate a single cell of lens epithelium.

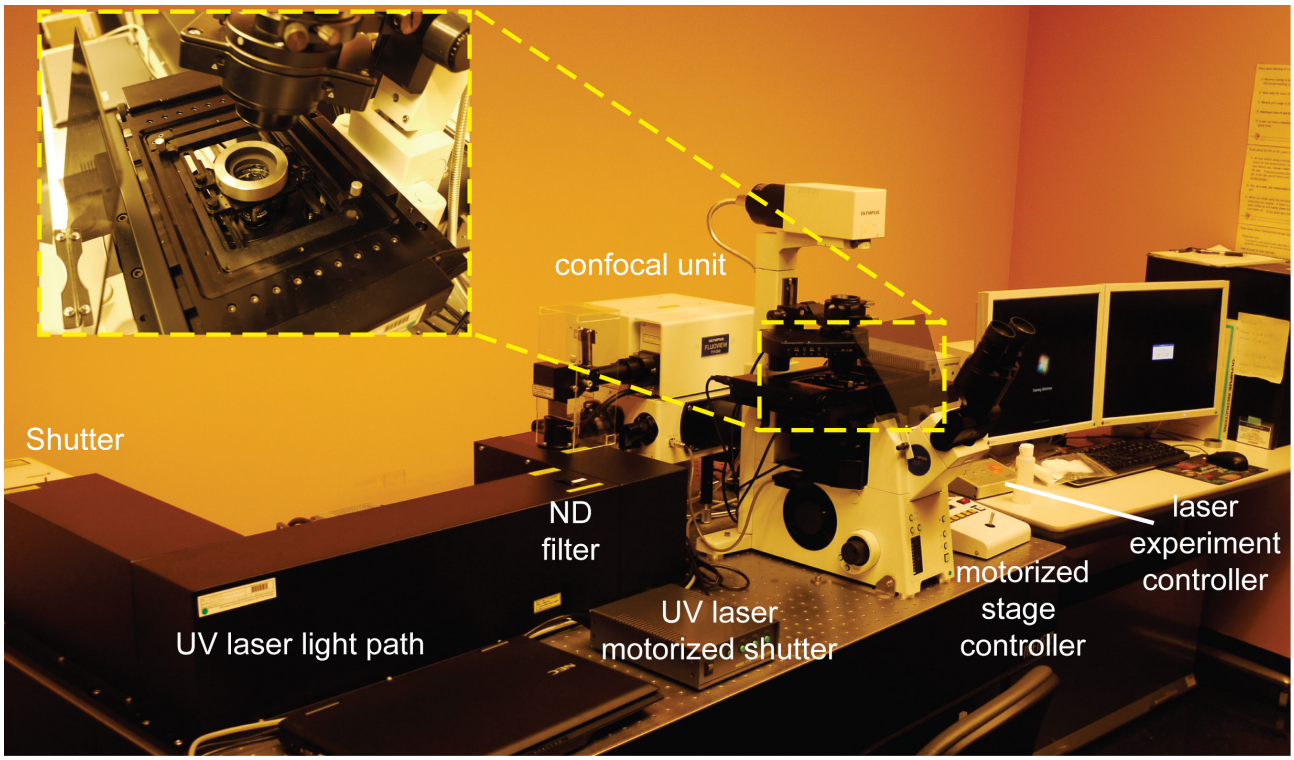

Figure S18. Configuration of the laser ablation system
Confocal laser scanning microscope (the right side of the image, FV1200, Olympus) combined with the UV ablation unit (the left side of the image). Inset indicates mounting of a zebrafish embryo on the stage. A glass dish containing a zebrafish embryo is held to the stage with putting a silver circle metal weight.

A

Laser setting output[%]	UPASAPO60x output[uJ] 20131030 ND 100	ND 50	ND 20	ND 5	ND 1
0					
10					
20					
30	–	–	–	–	–
35	0.21	–	–	–	–
40	0.21	–	–	–	–
45	0.44	0.26	–	–	–
50	0.75	0.42	0.20	–	–
55	1.09	0.61	0.27	–	–
60	1.54	0.83	0.36	–	–
65	2.10	1.13	0.46	–	–
70	2.58	1.39	0.57	0.20	–
75	3.04	1.65	0.66	0.23	–
80	3.58	1.96	0.78	0.26	–
85	4.26	2.31	0.92	0.29	–
90	4.80	2.62	1.05	0.33	–
95	5.40	2.94	1.17	0.36	–
100	5.94	3.23	1.27	0.39	–

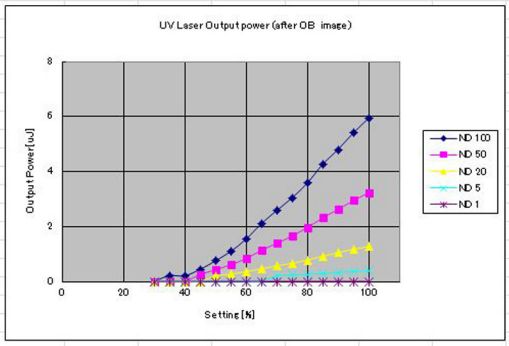

B

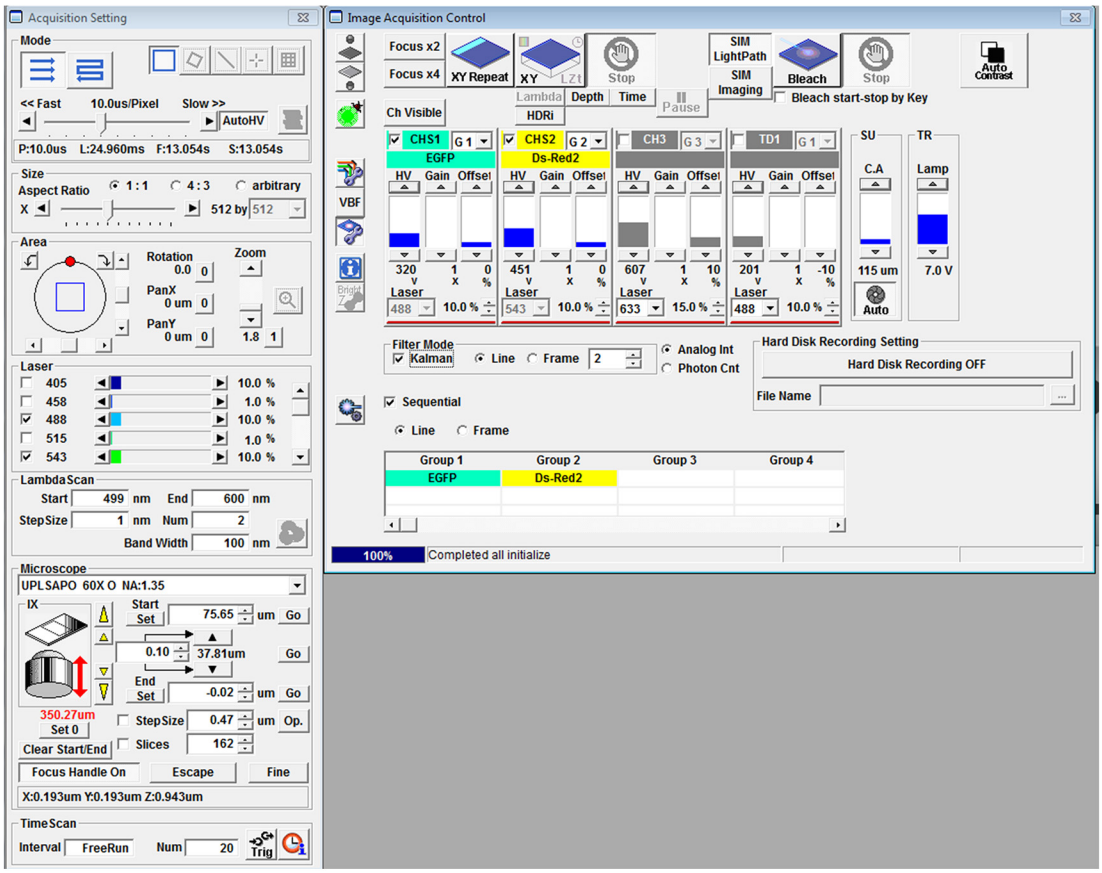

Figure S19. Setting parameters for the laser ablation experiment

(A) The relationship between actual laser power and laser setting output with different neutral density (ND) filter configurations profiled by the manufacturer. We selected 65-80% for laser setting output and an ND50 filter to obtain 1.13-1.96 μJ as the actual laser output at the focal point

(B) Screen shot image of the ablation experiment in FluoView.

Supplementary table I

sample	ND	DV (t=0)	eliminated	Total
WT1	31	21	7	59
WT2	24	19	2	45
WT3	26	21	1	48
WT4	27	12	14	53
WT5	36	16	2	54
E-cad1	43	17	16	76
E-cad2	30	11	5	46
E-cad3	27	8	2	37
N-cad1	30	24	15	69
N-cad2	25	26	3	54
N-cad3	28	18	1	47

Supplementary methods

Time lapse scanning and analysis of *Tg(h2afva:GFP; EF1α:mCherry-zGem) transgenic fish lens*

Zebrafish wild-type, E-cadherin mutant, and N-cadherin morphant embryos carrying the transgene *Tg(h2afva:GFP; EF1α:mCherry-zGem)* were produced and developed by 30 hpf in E3 embryonic medium containing 0.003% 1-phenyl-2-thiourea (PTU), which prevents melanin pigmentation. At 30 hpf, the chorion of embryos was removed, and after anesthetization in 200 mg/L Tricaine (3-amino benzoic acid ethyl ester, Sigma A-5040), embryos were mounted on a microscope stage. Configuration for sample mounting on a confocal laser scanning microscope (LSM) is shown in Fig. S12A–B. Since we used an upright LSM microscope, embryos were mounted on their sides in a groove stretched in an acrylic plate for positioning yolk with a drop of 3% methylene cellulose (Fig. S12C), and covered with 1% low-melting point agarose prepared in E3 medium within a strengthening ring (One-Patch Stamp; Kokuyo, PSM10B; outside diameter, 14.5 mm; inside diameter, 6 mm), which prevents detachment of the agarose from the acryl plate (Fig. S12D). After solidification of the agarose at room temperature, E3 medium with 200 mg/L Tricaine and 0.003% PTU was poured into the dish. Mineral oil was then layered on the E3 medium to prevent evaporation (Fig. S12A–B). Fish embryos were scanned on their sides using a Zeiss LSM confocal system in z-stack and time-series scanning mode (Fig. S12E). General parameters for confocal scanning as followings (Zeiss LSM 710 upright confocal system): Objective, W Plan-Apochromat 40x/1.0 DIC M27; Resolution, 512x512 pixels in 8-bit; Pinhole, 40–70 μm; Scanning mode, bidirectional and speed 6-7; Noise reduction, line 2 scan in median mode; Laser power, 488 nm 3–4%, 543 nm 10%; Master gain 1000–1100V; Digital Gain, 1.0; Digital offset, -10; Zoom, 1.0–1.3.

For time-lapse scanning with the confocal LSM, the region of interest of lens was first cropped using Zeiss imaging software, ZEN, to reduce the file size. Noise was reduced using a median filter. Time-lapse images were obtained every 15 min for 12 hr after 33 hpf. Scanned 3D time-lapse movies were analyzed with Imaris software (ver. 7.6.5, Bitplane). Drifting lens position during the scanned period was corrected using the "Drift Correction" tool of Imaris software, which selected one nucleus that showed no cell division and little or no movement within the most anterior area, as a steady-point reference and adjusted surrounding images relative to this reference (Fig. S13A–D). The volume of interest (VOI) of the lens was then cropped by drawing contour circles and by creating a surface that masked the lens (Fig. S13E–H). Next, the internal lens fiber area was cropped by drawing inside contour circles and by creating a surface that masked the lens fiber core (Fig. S13I–L). Throughout these processes, digitally resected lens epithelium was prepared (Fig. S13M–N), and its anterior lens epithelium was further extracted using Imaris "Ortho Slicer" tool (Fig. S13O–P) and used for epithelial cell movement tracking and behavior analysis.

After we obtained 3D time-lapse movies of five wild-type, three E-cadherin mutant, and three N-cadherin morphant lenses, cell lineages for each lens were traced with connecting nuclei between individual time-lapse images using the Imaris "Track Particles" tool with manual

correction (Fig. S13Q–S). All epithelial cells were classified as dividing, non-dividing and eliminated cell populations for each lens (Supplementary Table I), and the eliminated cell population was further classified into cells that underwent apoptosis or that simply moved out of the lens epithelium by monitoring whether chromatin collapsed when eliminated cell population disappeared, and these data were analyzed to calculate the fraction of these cell populations for each genotype (Fig. S1A–D and Fig. S2A). Next, using cell lineage data, cell movement speed, tracking length, and displacement length for each time frame were measured for each lineage of dividing and non-dividing cell population: especially, for dividing cell population, two daughter cell lineages were separately analyzed, and shown on trajectory maps (Fig. S13T–W). Average values of these parameters during the scanned period were calculated for each cell lineage from the Imaris Dataset, and average values of cell movement speed, tracking length, and displacement length for dividing and non-dividing cell populations were calculated for each lens using average values of each cell lineage. For analyses of cell movement parameters in cell-cycle phases, speed of cell movement on each time frame was manually calculated using cell position distance between the preceding and immediately following time frames. Cell-cycle phases of individual cells for each time frame were determined by fluorescent colors of *Tg(h2afva:GFP; EF1α:mCherry-zGem)*. Combined with this information, average speed of cells in G1, S/G2, and M phase were calculated for each lens.

For measurement of nuclear volume, objects demarcating the surface of GFP-labeled chromatin in the anterior lens epithelium were created for individual time-lapse movies, using the "surface rendering" tool of the Imaris software (Fig. S9A), and their volume were calculated. Ten lens epithelial cells were selected in the early stage of the scanned period (33–36 hpf) when no apoptotic cells were observed. The average value of epithelial nuclear volume was calculated using these ten samples for each lens (Fig. S9B). Five wild-type, three E-cadherin mutant, and three N-cadherin morphant lenses were used for evaluation of the difference in lens epithelial nuclear size for each genotype (Fig. S9C).

For time-lapse scanning of the equatorial region of the lens, the same time-lapse scanning procedure for the anterior lens epithelium was applied, except that embryos were mounted in a ventral view on a groove stretched in an acrylic plate. Drift movement was corrected using the most anterior lens epithelial cell that showed no cell division and little or no movement, as a steady-point reference and the lens was extracted by cropping the outside retina and cornea (Fig. S14A). Then, lens epithelium in the equatorial region was digitally resected by cropping the inside lens fiber cores (Fig. S14B–C) and using "Ortho slicer" tool (Fig. S14D).

Time lapse scanning and analysis of *Tg(h2afva:GFP; EF1α:mCherry-CAAX)* transgenic fish lens

Zebrafish wild-type and E-cadherin mutant embryos carrying the transgene *Tg(h2afva:GFP; EF1α:mCherry-CAAX)* were produced and developed by 30 hpf in E3 embryonic medium containing 0.003% PTU. Time-lapse images of the anterior lens epithelium from *Tg(h2afva:GFP;*

EF1α:mCherry-CAAX) fish were obtained using the same procedure as with *Tg(h2afva:GFP; EF1α:mCherry-zGem)* fish (Fig. S15A). After correcting for drift during scanning, the lens epithelium was cropped by drawing outer contours and by performing surface masking. The major reason for using *Tg(h2afva:GFP; EF1α:mCherry-CAAX)* was to obtain the information on the plasma membrane domain that is associated with adherens junctions for analyses of epithelial cell arrangement, such as cell intercalation. The most anterior region of lens epithelium usually consists of around eight confocal slices 1 μm thick along the AP axis, and among these eight slices, only one corresponds to the focal plane, which contains a plasma membrane domain that is associated with adherens junctions and is just adjacent to the anterior top of lens fiber core (Fig. S15B). Thus, we extracted such confocal images from a series of 3D z-axis stacked images using the "Ortho Slicer" tool or by selecting an appropriate confocal image slice for each of 15 min time point (Fig. S15C) and compiling them to make a time-lapse movie. Since the movie provides information on plasma membranes associated with adherens junctions, it is useful for studying cell intercalation. Individual cell lineages were traced with assignment identification numbers for each cell throughout the scanned period.

For evaluation of lens epithelial area expansion during development, we selected 10-15 cells in movies of the apical lens epithelial region for three wild-type and three *hab*^{rk3} mutant lenses, and calculated cell areas at each time point, using ImageJ. We also manually identified cell divisions and cell intercalations in each movie and examined temporal relationships between cell division and cell intercalation. Area expansion rate for each 15 min interval (% of original area size/min) was calculated. The average expansion rate was calculated for cell division period, cell intercalation period, and for the rest period when cell division and cell intercalation do not occur.

Determination of cell movement direction

Cell movement direction in the lens epithelium was calculated using time-lapse 3D images from an anterior view. In XYZ coordinates of time-lapse images after drift correction, the position of the reference nucleus, which corresponds to the anterior pole of the lens sphere, is defined as (0, 0, 0). When an epithelial cell (nucleus) moved from position (x_1, y_1, z_1) to (x_2, y_2, z_2) in the lens epithelium, the displacement vector X (x_d, y_d, z_d) was determined using the following equations: $x_d = x_2 - x_1$; $y_d = y_2 - y_1$; $z_d = z_2 - z_1$. We defined cell movement direction as the angle θ between the line from (x_1, y_1, z_1) to (x_2, y_2, z_2) and the circumferential line that crosses the initial cell position (x_1, y_1, z_1). To calculate θ, we defined vector A (a, b, 0) that is parallel to the circumferential line that crosses the initial cell position (x_1, y_1, z_1). The vector A (a, b, 0) should be perpendicular to a vector (x_1, y_1, 0) and calculated using the equation shown below (where $a^2+b^2=1$).

$$A(a, b, 0) = \left(\frac{y_1}{\sqrt{{x_1}^2 + {y_1}^2}}, \frac{x_1}{\sqrt{{x_1}^2 + {y_1}^2}}, 0\right)$$

Whereas θ is calculated using the equation below.

$$\cos\theta = \frac{|ax_d + by_d|}{|\vec{A}||\vec{X}|}$$

To determine cell movement direction along the AP axis, lens epithelial region was divided into sub-regions along the AP axis: r=0–6, 6–11, 11–16, 16–21, 21–26, 26–31 (μm). Lens epithelial cells positioned in each sub-region at the beginning of the scanned period (t=0) were identified and their displacement vectors from t=0 to t=735 min were determined. The vector A was also determined for each lens epithelial cell. Then, cell movement orientation θ was calculated using the equation above. The average of cell movement orientation θ was determined per sub-region of the AP axis in wild-type, E-cadherin mutant and N-cadherin morphant lenses and was plotted in the histograms shown in Fig. 1H, 3F and 4F, respectively.

The cell movement angle in the equatorial region was also defined as the angle between the displacement vector and the circumferential axis. In both cases, 0° was defined as circumferential movement and –90° as longitudinal movement toward the posterior pole.

Evaluation of cell clustering

We conducted cell clustering analyses at three time points during the scanned period: t=0, 360, and 735 min elapsed after 33 hpf. First, we determined the number of non-dividing, dividing and eliminated cell populations, which are defined as $N(t)_{ND}$, $N(t)_{DV}$, and $N(t)_e$, respectively, at the three time points in wild-type, E-cadherin mutant and N-cadherin morphant lenses. During the time-lapse scanning period (33–45 hpf), the eliminated cell population disappeared, whereas the dividing cell population doubled during one round of cell division. In accordance with our definition, cells that had not divided, but would undergo cell division later were pre-designated as belonging to dividing cell population even before the actual time of cell division. Similarly, cells that had not disappeared, but would be eliminated later were pre-designated as members of eliminated cell population before their actual time of cell elimination. Since almost all eliminated cells we observed in this analysis did not divide during scanning, we counted eliminated cell population as non-dividing cell population at t=0 and 360 for the classification of pentagonal cell cluster patterns. To determine the distribution pattern of pentagonal cell clusters in the random distribution model, we calculated the ratio of the number of non-dividing and dividing cell populations relative to total lens epithelial cells at each time point (t), $R_{ND}(t)$ and $R_{DV}(t)$, using the following equations.

$$\mathrm{R}(t)_{ND} = \frac{\mathrm{N}(t=33)_{ND} + \mathrm{N}(t)_e}{\mathrm{N}(t=33)_{ND} + \mathrm{N}(t)_e + \mathrm{N}(t)_{DV}}$$

$$\mathrm{R}(t)_{DV} = \frac{\mathrm{N}(t)_{DV}}{\mathrm{N}(t=33)_{ND} + \mathrm{N}(t)_e + \mathrm{N}(t)_{DV}}$$

Using images of *Tg(h2afva:GFP)*, we selected the five cells closest to the cell of interest, forming a virtual pentagon of surrounding cells. Pentagonal cell patterns are classified into six types depending on combinations of dividing and non-dividing cell numbers: type 1 (all 5 non-dividing cells), type 2 (4 non-dividing cells and 1 dividing cell), type 3 (3 non-dividing and 2 dividing cells), type 4 (2 non-dividing and 3 dividing cells), type 5 (1 non-dividing and 4 dividing cells) and type 6 (all 5 dividing cells). The probability of type n when a pentagonal pattern is generated by the random distribution, P_n, was calculated from the equation below.

$$P_n = C_{n-1}^{5} \times \mathrm{R}(t)_{ND}{}^{6-n} \times \mathrm{R}(t)_{DV}{}^{n-1}$$

The procedure for calculating the probability for each pentagonal pattern of a wild-type lens WT1 at 45 hpf was indicated as an example in Fig. S16A.

Next, to determine the distributional profile of dividing and non-dividing cell populations, we examined the pentagonal patterns of individual lens epithelial cells using schematic images representing non-dividing, dividing and eliminated cell populations as blue, yellow, and purple respectively (Fig. S16B), and determined the distribution profile of non-dividing and dividing cell populations. Distribution profiles of pentagonal clusters with a centered dividing cell population and a centered non-dividing cell population, and of the random distribution model are shown in the middle panel of Fig. 1E (WT1, t=735 min), the top panels of Fig. 3C (E-cad1, t=735 min) and Fig. 4C (N-cad1, t=735 min), and Fig. S3A (WT1~5, E-cad1~3, and N-cad1~3; t=0, 360 and 735 min). The average number of dividing cell population in pentagonal clusters for each lens and for each genotype was calculated and shown in Fig. S3B and S3C, respectively.

Laser ablation experiments

Zebrafish wild-type and E-cadherin mutant embryos carrying the transgene *Tg(h2afva:GFP; EF1α:mCherry-CAAX)* were produced and developed by 50 hpf in E3 embryonic medium containing 0.003% PTU. N-cadherin morphant embryos carrying the transgene *Tg(h2afva:GFP; EF1α:mCherry-CAAX)* were prepared by injection of MO-Ncad at 50 μM. At 50 hpf, embryonic chorions were removed and embryos were anesthetized in E3 embryonic medium containing 200 mg/L Tricaine. Embryos were mounted onto glass-bottom dishes (diameter 27mm, 3910-035, IWAKI, Japan) with a drop of 3% methylcellulose (M-0387, Sigma-Aldrich, USA), and oriented so that the eye was close to the bottom. 50 μL of 1.3% low-melting agarose buffered with E3 medium at 42 ºC was then added on top of the embryos to hold the embryo orientation. After solidification of the agarose, E3 medium containing Tricaine was added just before UV laser ablation. The workflow is shown in Fig. S17.

The UV laser ablation unit was combined with an inverted confocal laser scanning microscope (FV1200 on IX81 motorized microscope, Olympus, Japan) (Fig. S18). The UV laser unit was based on a solid-state, Q-switched, 349-nm UV laser with pulse width (FWHM) <5ns,

adjustable repetition rate up to 5 kHz, and maximum power up to 20 μJ (Explorer OEM, Explorer-349-120-1KE, Nd:YLF gain medium, Spectral Physics, USA). The microscope objective lens with high UV transmission (UPlanSAPO 60X Oil, NA=1.35, ∞/0.17/FN26.5, Olympus, Japan) was used. A glass bottom dish with a mounted fish embryo was put on the stage and held firmly by a weight (JA710800, Olympus) as shown in the inset of Fig. S18. The embryo was moved into the center of the view field so that the lens epithelial cell to be ablated was centered. A single laser shot with just enough power for single cell ablation was fired during the first few frames of time-lapse scanning of lens epithelium. In accordance with information on the relationship between actual laser power and laser setting output provided by the company (Fig. S19A), a Neural Density 50 (ND50) filter was used for all experiments. Laser output was set between 65-80%, so that the actual laser output at the focal point was 1.13-1.96 μJ. Parameters for the confocal microscope were as follows.

(1) Scanning speed: 10 μm/pixel
(2) Resolution: 512x512 pixels
(3) Magnification: 1.8X
(4) 488 nm & 543 nm laser power: 10%
(5) Gain: 1X
(6) Kalman Filter:2
(7) Sequential line scanning
(8) Without differential interference contrast
(9) Acquisition interval: 15 seconds

Screenshot pf the ablation experiment in FluoView of FV1200 is shown in Fig. S19B.
Using ImageJ software, the ablated area was analyzed.

Movies

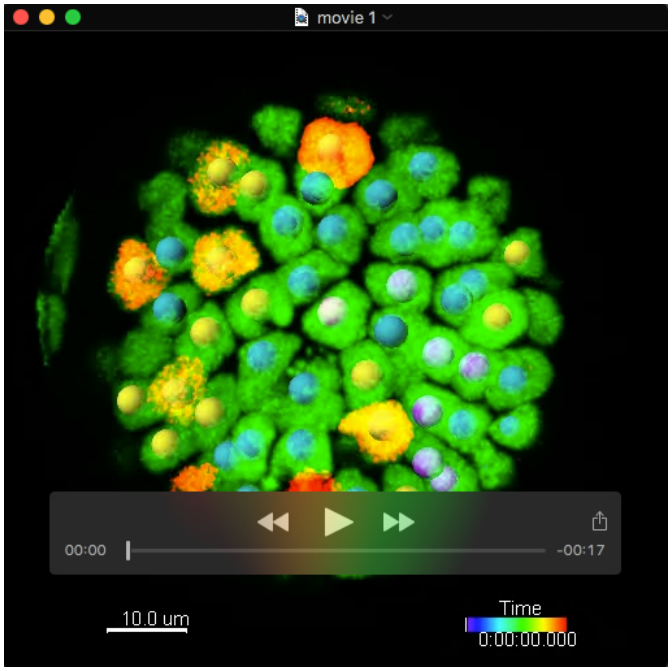

Movie 1

Time-lapse movie of the anterior region of wild-type lens epithelium combined with a zebrafish transgenic line *Tg(h2afva:GFP; EF1α:mCherry-zGem)* from 33 to 45 hpf. Green and red fluorescence indicates cells undergoing the G1 and the S/G2/M phase, respectively. In M phase, chromatin labeled in green fluorescence is condensed. Movie images are associated with spot representation, in which dividing, non-dividing, and eliminated cell populations are indicated by yellow, blue, and purple, respectively. Spot colors are based on the rule by which dividing and eliminated cells were marked beforehand, prior to cell division and cell elimination, respectively.

Movie 2

Time-lapse movie of the most apical region of wild-type lens epithelium combined with a zebrafish transgenic line *Tg(h2afva:GFP; EF1α:mCherry-CAAX)* from 33 to 45 hpf.

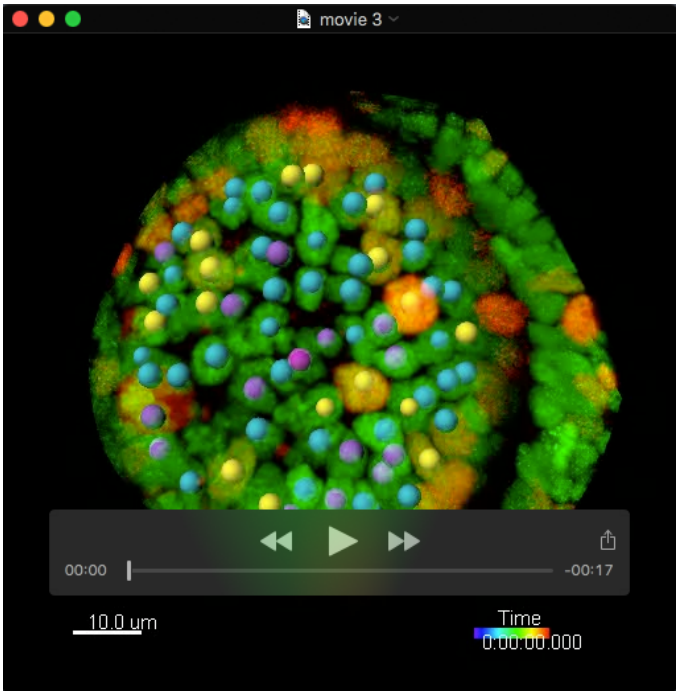

Movie 3

Time-lapse movie of the anterior region of E-cadherin mutant lens epithelium combined with a zebrafish transgenic line *Tg(h2afva:GFP; EF1α:mCherry-zGem)* from 33 to 45 hpf. Movie images are associated with spot representation, in which dividing, non-dividing, and eliminated cell populations are indicated by yellow, blue, and purple, respectively.

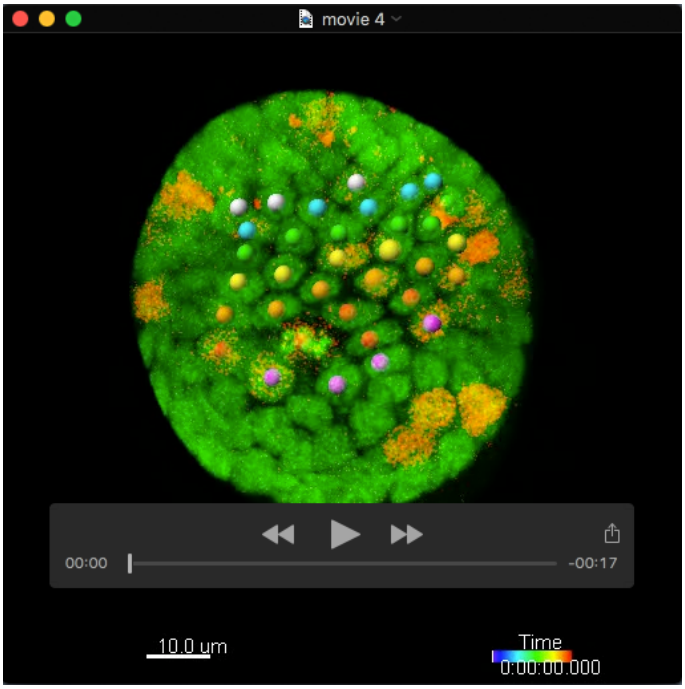

Movie 4

Time-lapse movie of the equatorial region of wild-type lens epithelium combined with a zebrafish transgenic line, *Tg(h2afva:GFP; EF1α:mCherry-zGem)* from 33 to 45 hpf. Different cell rows are indicated by color: Row 0, white; Row 1, light blue; Row 2, green; Row 3, yellow; Row 4, orange; Row 5, red; and Row 6, pink.

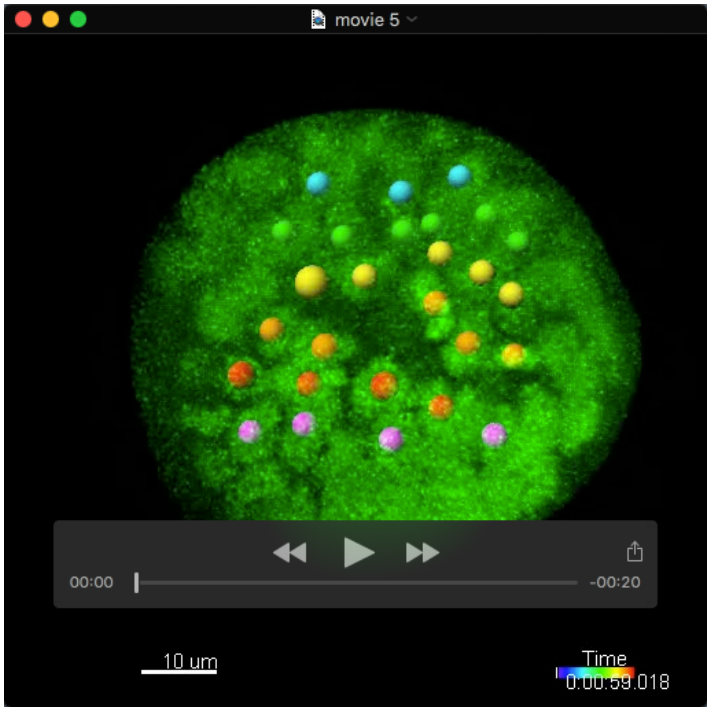

Movie 5

Time-lapse movie of the equatorial region of E-cadherin mutant lens epithelium combined with a zebrafish transgenic line, *Tg(h2afva:GFP)* from 33 to 45 hpf. Different rows of cells are indicated by color: Row 1, light blue; Row 2, green; Row 3, yellow; Row 4, orange; Row 5, red; Row 6, pink.

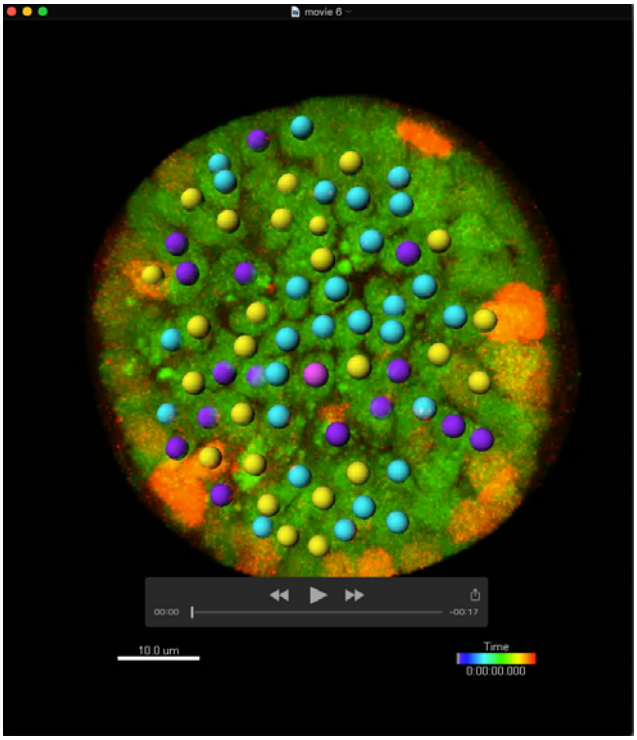

Movie 6

Time-lapse movie of the anterior region of *N-cadherin* morphant lens epithelium combined with a zebrafish transgenic line *Tg(h2afva:GFP; EF1α:mCherry-zGem)* from 33 to 45 hpf. Movie images are associated with spot representation, in which dividing, non-dividing, and eliminated cell populations are indicated by yellow, blue, and purple, respectively.

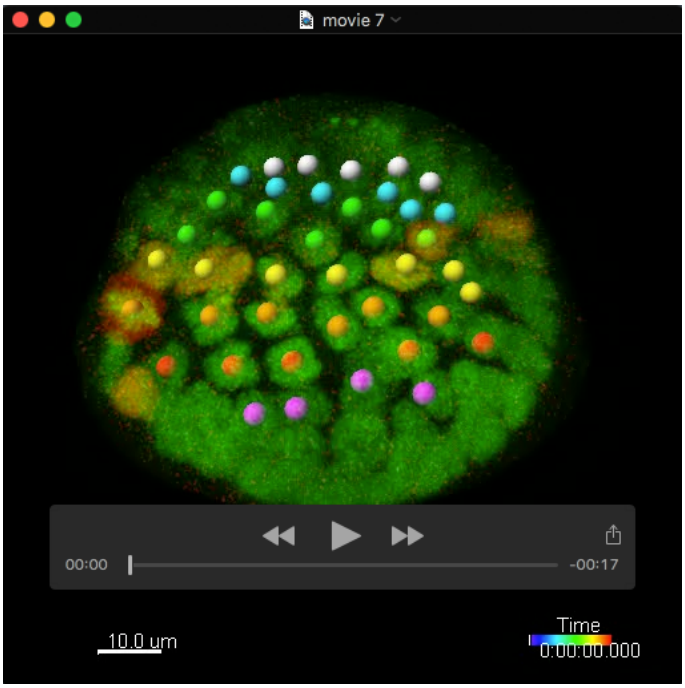

Movie 7

Time-lapse movie of the equatorial region of an *N-cadherin* morphant lens epithelium combined with a zebrafish transgenic line *Tg(h2afva:GFP; EF1α:mCherry-zGem)* from 33 to 45 hpf. Different rows of cells are indicated by color: Row 0, white; Row 1, light blue; Row 2, green; Row 3, yellow; Row 4, orange; Row 5, red; and Row 6, pink.

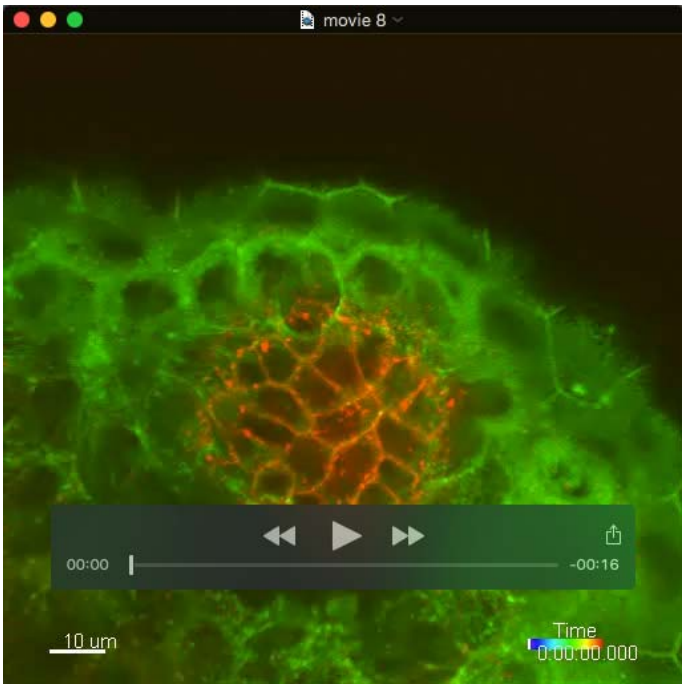

Movie 8

Time-lapse movie of the anterior region of 50 hpf wild-type lens epithelium combined with a zebrafish transgenic line, *Tg(actb1:myl12.1-eGFP; EF1α:mCherry-CAAX)* after the laser ablation.

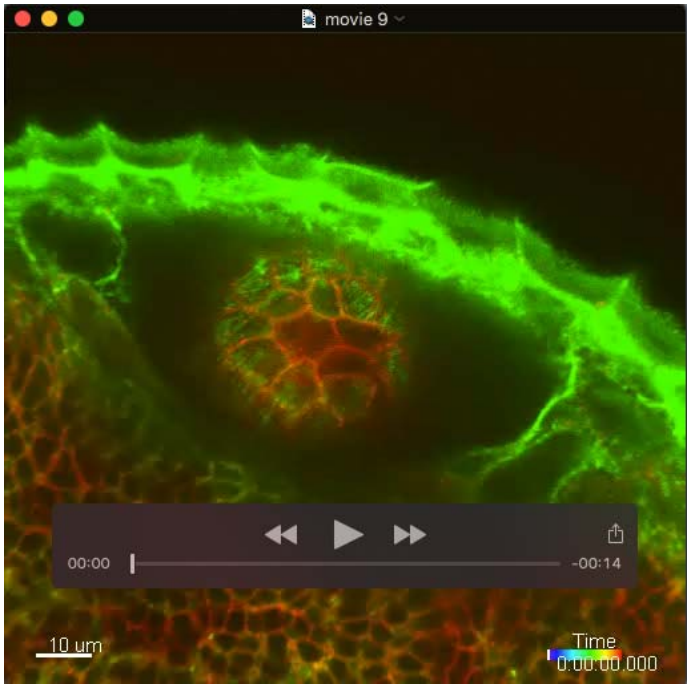

Movie 9

Time-lapse movie of the anterior region of 50 hpf *E-cadherin* morphant lens epithelium combined with a zebrafish transgenic line, *Tg(actb1:myl12.1-eGFP; EF1α:mCherry-CAAX)* after laser ablation.

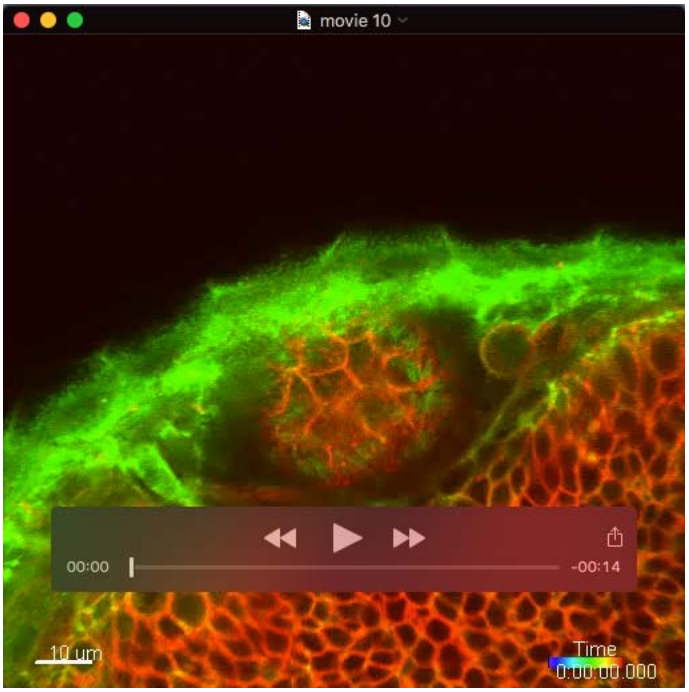

Movie 10

Time-lapse movie of the anterior region of 50 hpf *N-cadherin* morphant lens epithelium combined with a zebrafish transgenic line, *Tg(actb1:myl12.1-eGFP; EF1α:mCherry-CAAX)* after laser ablation.